Climate variability, heat distribution and polar amplification in the warm unipolar 'icehouse' of the Oligocene

Dominique K.L.L. Jenny[1], Tammo Reichgelt[2], Charlotte L. O'Brien[3], Xiaoqing Liu[4], Peter K. Bijl[1], Matthew Huber[4], Appy Sluijs[1]

[1] Department of Earth Sciences, Utrecht University, 3584 CB, Netherlands
[2] Department of Earth Sciences, University of Connecticut, CT 06269-1045, USA
[3] Department of Geography, University College London, WC1E 6BT, UK
[4] Department of Earth, Atmospheric, and Planetary Sciences, Purdue University, IN 47907, USA

Correspondence to: Dominique K.L.L. Jenny (d.k.l.l.jenny@uu.nl)

Abstract

The Oligocene (33.9 – 23.03 Ma) had warm climates with flattened meridional temperature gradients, while Antarctica retained a significant cryosphere. These may pose imperfect analogues to distant future climate states with unipolar icehouse conditions. Although local and regional climate and environmental reconstructions of Oligocene conditions are available, the community lacks synthesis of regional reconstructions. To provide a comprehensive overview of marine and terrestrial climate and environmental conditions in the Oligocene, as well as a reconstruction of trends through time, we here review marine and terrestrial proxy records and compare these to numerical climate model simulations of the Oligocene. Results, based on the present relatively sparse data suggest similar-to-modern temperatures around the equator. Sea surface temperatures (SSTs) show patterns similar to land temperatures, with warm conditions at mid and high latitudes (~60 – 90°), especially in the Southern Hemisphere. Vegetation-based precipitation reconstructions of the Oligocene suggest regionally drier conditions compared to modern times around the equator. When compared to proxy data, climate model simulations overestimate Oligocene precipitation in most areas, particularly the tropics. Temperatures around the mid to high latitudes are generally underestimated in models compared to proxy data and tend to overestimate the warming in the tropics. In line with previous proxy to model comparisons, we find that models underestimate polar amplification and overestimate the equator-to-pole temperature gradient suggested from the available proxy data. This further stresses the urgency of solving this widely recorded problem for past warm climates, such as the Oligocene.

1 Introduction

Simulations of future climate change, by current generation fully coupled climate models, indicate that global average surface warming will continue over the coming centuries depending on future CO_2 emissions and sequestration (IPCC, 2022). The models, as well as available temperature, CO_2 and sea level reconstructions of past Mesozoic and Cenozoic warm climates, suggest that Earth's climate may ultimately move towards unipolar conditions, with ice only remaining on Antarctica (Burke et al., 2018; Clark et al., 2016). Climate models additionally predict a global equilibrium surface warming between 1.5–4.5°C per doubling of atmospheric CO_2 concentrations relative to pre-industrial values, most likely with a value around 3 °C (IPCC, 2022). This warming will be amplified at higher latitudes, notably the Arctic, by a factor of 2–3 relative to the global average (Fischer et al., 2018; Holland and Bitz, 2003; IPCC, 2022). However, model projections, particularly for such distant future non-analogue states, still include large uncertainties and are ideally independently constrained by data. Proxy-based reconstructions of past climates provide useful insights into the Earth's natural response to CO_2 changes and therefore are an independent opportunity to quantify the sensitivity of various climate parameters to greenhouse forcing, including sea-level and polar amplification (e.g., Burke et al., 2018; Lunt et al., 2016; Palaeosens Project Members, 2012). This way, climate models which are simulating past climate conditions can be compared against proxy data, hence the performance of the models can be evaluated.

It is likely that important climate parameters such as equilibrium climate sensitivity and polar amplification depend on the state of the climate (e.g., Farnsworth et al., 2019; Gaskell et al., 2022; Hutchinson et al., 2021; Köhler et al., 2015; Masson-Delmotte et al., 2013). Therefore, these parameters have been investigated for several past climate states. Traditional targets include the Pleistocene, Pliocene and Eocene (e.g., Burke et al., 2018) and, more recently, the Miocene (Steinthorsdottir et al., 2021). These time intervals encompass a wide range of climate states, including those with ice sheets in both the Southern (SH) and Northern Hemisphere (NH), the Southern Hemisphere only, and ice-free states, in addition to a wide range of atmospheric greenhouse gas concentrations (e.g., Rae et al., 2021).

Recent work (e.g., O'Brien et al., 2020) has highlighted the Oligocene as a potentially useful climate state which allows to assess the dynamics of global climate with only an Antarctic ice sheet present. Though geographical boundary conditions during the Oligocene (33.9–23.03 million years ago (Ma)) were different to today, along with the Miocene, the Oligocene is a useful and relatively recent analogue to future unipolar icehouse climate states (e.g., O'Brien et al., 2020; Liebrand et al., 2017; Miller et al., 1988). Sparse glacially deposited sediments suggest the presence of NH glaciers as young as the late Eocene (Eldrett et al., 2007; St. John, 2008), but there is no evidence for late Eocene large-scale continental glaciation. Instead, the cryosphere potentially comprised localized glaciers and restricted sea ice in the Arctic Ocean (DeConto et al., 2008; Stickley et al., 2009). Reconstructions of atmospheric CO_2 range from over 1000 parts per million (ppm) to as low as ~300 ppm for the Oligocene (Foster et al., 2017; Rae et al., 2021), similar to the range projected for the future based on various emission scenarios (IPCC, 2022). Despite potentially low atmospheric CO_2 conditions, the few available sea surface temperature (SST)

reconstructions indicate warmer than modern climates throughout the Oligocene, with remarkable polar amplification (O'Brien et al., 2020).

Across the Eocene-Oligocene transition (EOT), atmospheric CO_2 concentrations dropped from >1000 ppm during the Eocene (56.0–33.9 Ma) to ~750 ppm or lower at the beginning of the Oligocene (Heureux and Rickaby, 2015; Pagani et al., 2005; Pearson et al., 2009). This drop coincides with a large increase (~1–1.5 ‰) in deep ocean benthic foraminifer oxygen isotope ratios ($\delta^{18}O$), which includes the effects of both the formation of ice sheets and a drop in deep-sea temperatures (e.g., Coxall & Wilson, 2011). The forcings underlying the onset of the Oligocene so-called 'icehouse' climate (i.e., with polar ice) are still highly debated. As of now the leading hypothesis invokes a strongly non-linear response to orbital forcing superimposed on a long-term drop in atmospheric CO_2 levels across a critical threshold (DeConto et al., 2008; DeConto and Pollard, 2003; Galeotti et al., 2016). However, the question that remains is if, or to what extent, tectonic changes and associated oceanographic reorganizations in the Southern Ocean (SO) played a role (e.g., Hill et al., 2013; Houben et al., 2019; Huber et al., 2004; Ladant et al., 2014; Sauermilch et al., 2021). Changes associated with the onset of polar glaciation include a drop in the global average temperature (Eldrett et al., 2009; Kotthoff et al., 2014; Liu et al., 2009; Meckler et al., 2022; Sluiter et al., 2022; Thompson et al., 2021; Zanazzi et al., 2007) and a profound change in deep-water temperatures (Meckler et al., 2022). Across the EOT, surface cooling (Liu et al., 2009), the accumulation of land ice that reached the Antarctic coastlines (Salamy and Zachos, 1999), and the consequent appearance of sea ice (Houben et al., 2013), were associated with pronounced changes in SH atmospheric circulation and oceanographic conditions (Diester-Haass & Zahn, 1996; Houben et al., 2019; Liu et al., 2009; Tripati et al., 2005) and an increase in the poleward ocean heat transport (Goldner et al., 2014). Global change at the beginning of the Oligocene also influenced the global turnover of flora and fauna (e.g., Solé et al., 2020; Sun et al., 2014). Oceanographic changes, including upwelling and the formation of sea ice, rapidly transformed circum-Antarctic marine ecosystems to such an extent, they may have influenced the evolution of large animal groups, such as the diversification amongst odontocete and mysticete (baleen) whales (e.g., Fordyce, 1980; Salamy and Zachos, 1999; Houben et al., 2013). Thus, the EOT seems to mark a prominent change in the global climate system (Westerhold et al., 2020) as continental ice sheets expanded.

Although the Oligocene has been the subject of numerous studies, the documentation of global Oligocene climate conditions and its variability, including the hemispheric distribution of heat, meridional temperature gradients, and biotic change is sparse and greatly relies on benthic foraminifer isotope data. With the Earth's high latitude cryosphere and climate directly responding to astronomical insolation changes, astronomical forcing studies of high-resolution benthic foraminifer $\delta^{18}O$ records are of great importance. Those studies (e.g., De Vleeschouwer et al., 2017; Galeotti et al., 2016; Levy et al., 2019; Liebrand et al., 2017; Naish et al., 2001; Pälike et al., 2006b) suggest significant variability in continental ice volume, paced by eccentricity and obliquity. Multiple-proxy SST data, albeit of much lower resolution than the deep ocean $\delta^{18}O$ records, revealed that the Oligocene was characterised by generally warm climates, with flattened meridional temperature gradients (Gaskell et al., 2022; O'Brien et al., 2020). Still, Antarctica retained a significant cryosphere (e.g., Hoem et al., 2021). The recorded trends, cycles and events provide ample opportunity to study the dynamics of climate and the carbon cycle in what has been called a 'doubthouse' or 'intermediate' climate state (O'Brien et al., 2020).

In this paper, we aim to review the current state of knowledge regarding the Oligocene climate to provide a baseline for focused future research. To this end, we first provide basic constraints regarding important climatic boundary conditions, such as paleogeography and atmospheric CO_2 levels. Additionally, a review of marine and terrestrial climate proxy records is presented, building on the compilation of marine records by O'Brien et al. (2020), to assess long term trends and variability in the Oligocene climate. The temperature and precipitation data were subsequently compared to the results of two sets of Oligocene climate model simulations to evaluate how well we understand the data from a climate physics point of view. Lastly, we identify specific points of interest for follow up research.

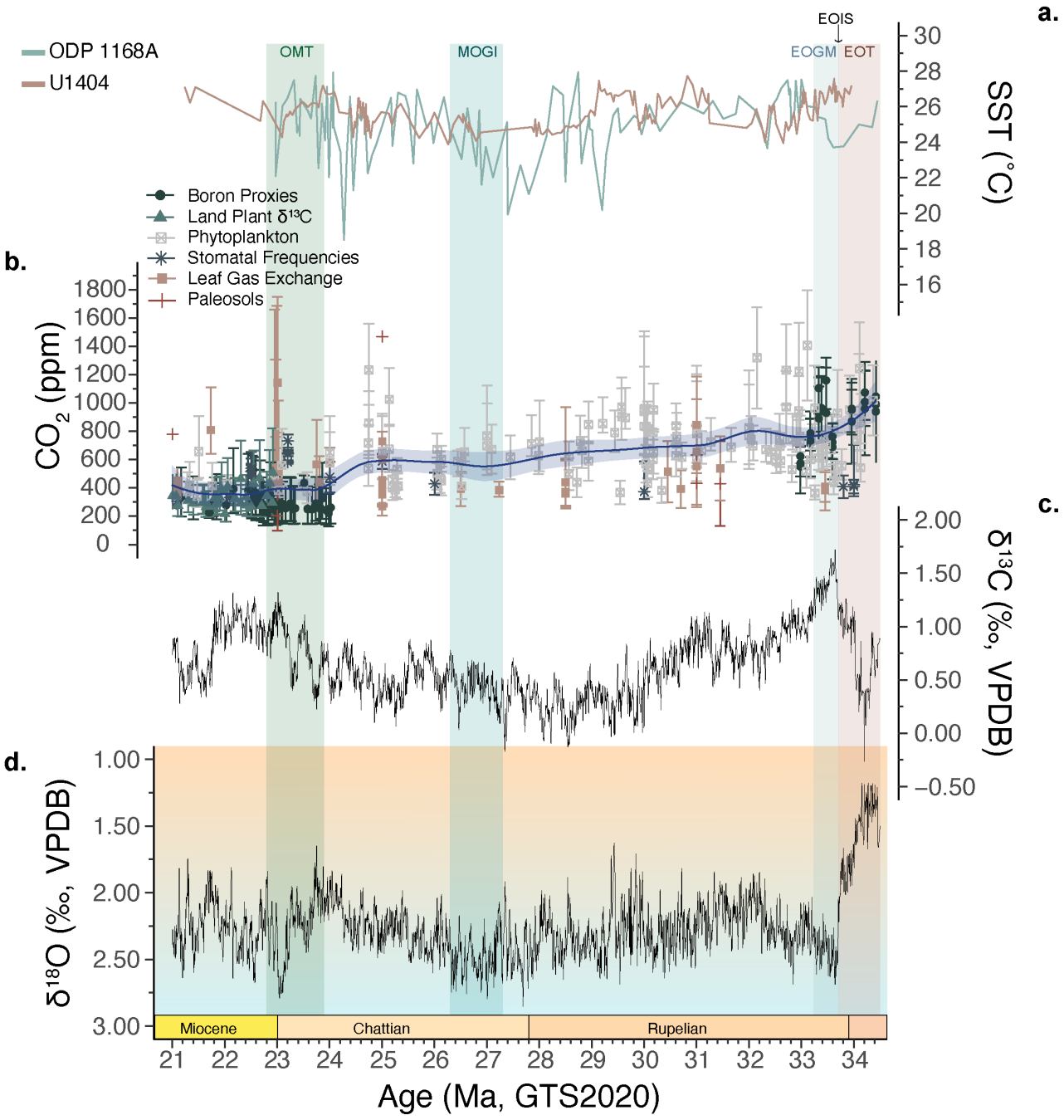

Figure 1: a. In blue: SST of ODP 1168A (west of Tasmania, TEX_{86}^{H}, Guitián & Stoll, 2021; Hoem et al., 2021) and in brown: SST of U1404 (northwest Atlantic, Uk37, Liu et al., 2018) b. Published pCO_2 records of the Oligocene, dark blue line and shading represents the median and 95% credible interval. Grey squares: phytoplankton data, brown squares: leaf gas exchange reconstructions, black dots: boron isotopic data, green triangles: land plant $\delta^{13}C$ data, brown crosses: palaeosol data, green stars: stomatal frequency data (Greenop et al., 2019; Moraweck et al., 2019; Pagani et al., 2005, 2011; Roth-Nebelsick et al., 2014; Witkowski et al., 2018; Zhang et

al., 2013; The Cenozoic CO2 Proxy Integration Project (CenCO2PIP) Consortium, 2023) c, d. Deep ocean benthic foraminifera stable carbon isotope and oxygen isotope records, respectively (Westerhold et al. 2020, notably representing the record of Pälike et al., 2006). Colour block red: Eocene-Oligocene Transition (EOT), grey: Eocene-Oligocene Glacial Maximum (EOGM), blue: Middle Oligocene Glacial Interval (MOGI), green: Oligocene-Miocene Transition (OMT).

2 Oligocene stratigraphical and chronological framework

2.1 Oligocene chronostratigraphy

The Oligocene represents the epoch between two formal Global Stratotype Section and Points (GSSP), the Eocene-Oligocene Boundary (EOB) and the Oligocene-Miocene Boundary (OMB), at 33.9 Ma and 23.04 Ma following the GTS2020 time scale (Gradstein et al., 2020). The EOB GSSP was set in 1992, at the Massignano Quarry (Italy) and is defined by the extinction of the two planktic foraminifer genera *Hantkenina* and *Cribrohantkenina* at 33.9 Ma (Silva and Jenkins, 1993). The GSSP for the OMB was defined by Steininger et al., (1997) in the Piedmont Tertiary Basin in Italy on the magnetic reversal from polarity chron C6Cn.2r–C6Cn.2n between two subunits of the Rigoroso Formation. Later Beddow et al., (2018) dated the base of C6Cn.2n at 23.040 Ma. Within the Oligocene, Hardenbol & Berggren (1978) were the first to distinguish the Rupelian (33.9–27.29 Ma) from the Chattian (27.29–23.040 Ma) of northwestern Europe. They separated the two periods based on lithostratigraphy in Belgium, into an open marine, clayey unit which overlies a shallower marine, sandy unit. The Rupelian (Chron C13r–C9n) was introduced by Dumont (1849), describing the Boom Clay Formation along the river Rupel and Scheldt in Belgium. The Chattian (Chron C9n–C6Cn) was officially first mentioned by Fuchs, (1894) who studied the "Kasseler Meeressande" (marine sands) in Hessen as well as Bünde, Germany (De Man et al., 2010; Van Simaeys, 2004; Van Simaeys et al., 2004). The GSSP for the Rupelian–Chattian boundary was set in 2016 by Coccioni et al., (2018) at the Monte Cagnero section near Urbania (Italy) and was bound by the (highest) last common occurrence (LCO) of the planktonic foraminifer *Chiloguembelina cubensis* at the base of the planktonic foraminifer zone O5. Currently, the official GSSP age for the Rupelian–Chattian boundary is 27.29 Ma, after Coccioni et al. (2018).

2.2 Oligocene Isotope Stratigraphy

Several informal definitions are used to describe the various stratigraphic isotope events associated with the Oligocene (Fig. 1). The Eocene-Oligocene transition (EOT) refers to the numerous climatic and environmental events broadly associated with the Epoch boundary (e.g., Coxall & Pearson, 2007; Eldrett et al., 2009; Houben et al., 2012; Zanazzi et al., 2007). However, Hutchinson et al. (2021) recently defined it as the ~790 kyr interval between the extinction of the coccolithophore species *Discoaster saipanensis* (~34.46 Ma) and the Earliest Oligocene Oxygen Isotope Step (EOIS). Hutchinson et al. (2021) also defined several other globally recognizable Oligocene isotope events, together replacing the classic Oligocene oxygen isotope zones of Miller et al. (1991). The EOIS — previously known as the onset of Oligocene oxygen isotope zone 1 (Oi-1; Miller et al., 1991) — is a ~40 kyr long lasting ≥0.7‰ $\delta^{18}O$ increase (Coxall & Wilson, 2011; Zachos et al., 1996) which peaks at ~33.71 Ma. The EOT and the EOIS are followed by the Early Oligocene Glacial Maximum (EOGM), which lasted ~490 kyr from ~33.71 to ~33.22 Ma and chronostratigraphically correlates to most of the geomagnetic polarity time scale (GPTS)

Magnetochron C13n (33.726–33.214 Ma) (Hutchinson et al., 2021). The EOGM was first introduced by Liu et al. (2004) and spans the separate $\delta^{18}O$ maxima which were defined by Zachos et al. (1996) as Oi-1a (~33.66 Ma) and Oi-1b (~33.26 Ma), a consecutive period of colder climate and/or glaciation. The Mid-Oligocene Glacial Interval (MOGI) represents a ~1 Myr long phase of strong variability in $\delta^{18}O$ with marked maxima representing profound cooling/glacial expansion between 27.3 and 26.3 Ma (Liebrand et al., 2017), previously referred to as Oi-2b. The MOGI was followed by three warming phases (~26.3, ~25.5 and ~24.22 Ma), after which cooling lead up to the Oligocene-Miocene transition (OMT, 23.88–23.04 Ma). The beginning of the Miocene (23.040–5.33 Ma) is marked by a ~1 ‰ rise in deep ocean benthic foraminifer $\delta^{18}O$ values, traditionally referred to as the Mi-1 event (Billups et al., 2002; Flower et al., 1997; Miller et al., 1991).

3. Boundary Conditions for Oligocene climate

3.1 Geographical Boundary Conditions

Oligocene plate tectonic geography differed from the modern configuration regarding several regions that are relevant to climate (Fig. 2). Specifically, plate tectonic movements may have been important for oceanographical change, influencing regional climate through changes in meridional and zonal heat transport. We here discuss the most prominent tectonic differences.

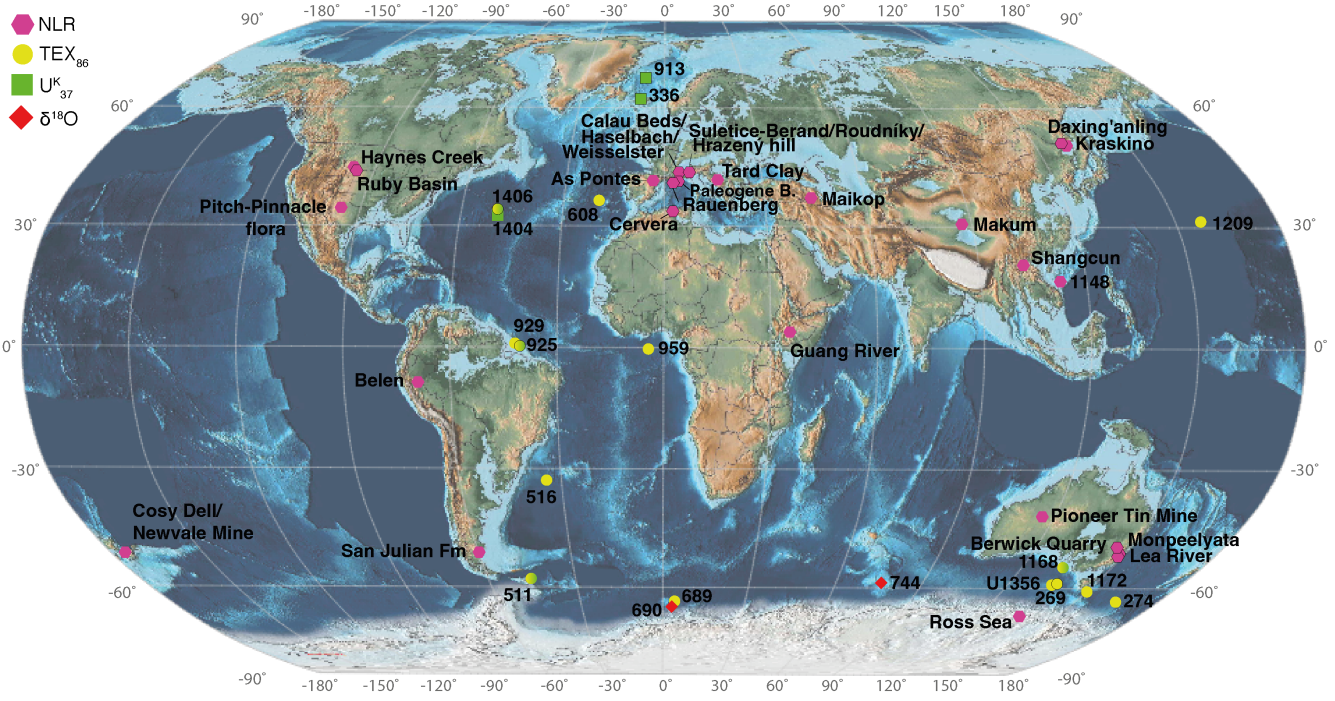

Figure 2: Paleogeographic reconstruction of the Oligocene (~28 Ma). Yellow dots: Tex_{86} based data; purple hexagons: Nearest Living Relative (NLR) data; green squares: U^{K}_{37} data; red diamonds: $\delta^{18}O$ data. Map created using Gplates, using the Scotese & Wright (2018) plate rotation.

One of the most discussed tectonic changes since the Oligocene is the uplift of the Tibetan Region (consisting of the Tibetan Plateau, the Himalaya and the Hengduan Mountains). Although the collision between India and the Eurasian plate predates the Oligocene (60–50 Ma; van Hinsbergen, 2022; Wang et al., 2014), continued collision created further uplift of the Himalaya and the Tibetan Plateau also in the Oligocene. The climatic consequences of the uplift are investigated both regionally (e.g., SE Asia; Ding et al., 2017; Su et al., 2019) and globally as a source of chemical weathering during the Cenozoic (e.g., Raymo & Ruddiman, 1992). Today the Tibetan Region has an average elevation of over 4.5km. During the Oligocene the elevation of the Tibetan Region was between 2.3 and 3km, with central Tibet most likely at similar altitudes as today (Spicer et al., 2020, 2021a, b; Su et al., 2019).

Another important tectonic event during the Oligocene was the convergence of the European and Adriatic plate which led to the formation of the Alpine system. While the collisional stage of the Alps began in the earliest Paleocene (65 Ma), during the Oligocene a slab from the subducted oceanic European lithosphere broke off, which resulted in the rapid and continued uplift of the Alps, which lasted until today but became stable in the mid Miocene (Meschede and Warr, 2019). This resulted in an Oligocene uplift of ~1km of the Alpine area, from an average elevation of <1km to 2km (Dielforder, 2017; Winterberg et al., 2020). Due to the strong tectonic changes around the eastern Alps and the Tibetan Region during the Oligocene, the so called 'Paratethys' (Laskarev, 1924), which reached from the western Molasse Basin in Switzerland to lake Aral between Kazakhstan and Uzbekistan, became a semi-isolated inland sea at the beginning of the Oligocene (Schulz et al., 2005; Steininger and Wessely, 1999). The Paratethys consisted of a series of adjacent sedimentary basins, of which the interconnections were rather unstable resulting in the separation of the Paratethys into three main parts: the Western (Alpine), Central (Balkan) and Eastern (Caucasian) Paratethys (Kováč, 2017; Palcu and Krijgsman, 2023; Rögl, 1998). A connection to the Mediterranean might have been established in the late Oligocene, connecting the Paratethys to the main oceans (Kováč, 2017).

Oceanic gateways in the Southern Ocean, including the Drake Passage (DP) and the Tasmanian Gateway, underwent tectonic changes in the Paleogene that were originally hypothesized to have strongly affected regional ocean circulation and associated heat and salt transport, as inferred from sedimentary data (e.g., Kennett, 1977; Murphy & Kennett, 1986). However, based on model simulations and biogeography the extent to which the opening of these gateways affected Cenozoic cooling, either globally or regionally, remains the subject of debate (Houben et al., 2019; Huber et al., 2004; Kennett, 1977; Sauermilch et al., 2021; Scher and Martin, 2006; Toumoulin et al., 2020). While exact age estimates for the first opening of the DP lay most likely in the middle to late Eocene (~50 Ma; Eagles and Jokat, 2014), it remains likely that the DP opened once or experienced intermittent closures that resulted in staggered throughflow over several tens of millions of years (van de Lagemaat et al., 2021).The DP opened due to tectonic processes between the South American, the Antarctic and the Central Scotia Plate (Eagles, 2016), and involved a complex opening of isolated ocean basins, which became oceanographically connected into one deep throughflow during the Oligocene (~26 Ma; van de Lagemaat et al., 2021). During the early to middle Oligocene (34–26 Ma), subduction initiated between South America and the Scotia Plate (Crameri et al., 2020), which led to the opening and deepening of several ocean basins in the area between 29.5 and 21.2 Ma (van de Lagemaat et al., 2021). This tectonic development facilitated the formation of a deeper DP gateway (Maldonado et al., 2014).

Although spreading between Australia and Antarctica initiated in the Cretaceous, the South Tasman Rise connected the continents until the latest Eocene (see overview in Bijl et al., 2021). Dinoflagellate cyst biogeographical evidence suggests shallow water connections between the Australo-Antarctic Gulf and the southwest Pacific initiated close to the early–middle Eocene transition (Bijl et al., 2013). Lithological evidence for rapid deepening of the South Tasman Rise at ~35.7 Ma (Stickley et al., 2004) was later found to be a Southern Ocean-wide phenomenon related to the initiation of the throughflow of a vigorous Antarctic Counter Current, and a proto-Antarctic Circumpolar Current (Houben et al., 2019). It is generally accepted that the Tasmanian Gateway was open to deep waters by Oligocene times (Stickley et al., 2004) but the Australian continent obstructed the optimal flow of strong circumpolar ocean currents until the late Neogene (Evangelinos et al., 2022; Hill et al., 2013; Sauermilch et al., 2021).

3.2 Ocean Circulation

Using marine magnetic data, Barker & Burrell (1977) found that the opening of the Southern Ocean gateways (SOG) (i.e., Drake Passage and the Tasmanian gateway) preconditioned the formation of the Antarctic Circumpolar Current (ACC) between Antarctica, South America, and Australia. As Earth's strongest ocean current, the modern ACC is not only responsible for the regulation of heat and carbon exchange from and to the atmosphere, but it also influences deep-water formation and nutrient distribution (Cox, 1989; Scher et al., 2015). The ACC encircles Antarctica and in doing so connects the deep waters of the Pacific, Indian and Atlantic Ocean. Models using middle Eocene to early Oligocene geographies and CO_2 values have sought to understand the influence of the SOG openings on the global ocean (e.g., Goldner et al., 2014; Hutchinson et al., 2018; Kennedy et al., 2015; Kennedy-Asser et al., 2019; Sauermilch et al., 2021; Baatsen et al., 2016). Model simulations suggest that as soon as the DP opened, a weak current (the proto-ACC) from the Pacific to the Atlantic would have established (Ladant et al., 2014). Additionally, the coupled model of Toggweiler & Bjornsson (2000) shows that winds around Antarctica raise cold dense water, cooling the region. This upwelled water then becomes fresher and warmer as it moves northwards due to Ekman transport. North of the ACC this lighter and warm water is transported downwards into the thermocline. This thickens the lower thermocline and creates a bigger density contrast across the Icelandic sills, ultimately enhancing the formation of North Atlantic Deep Water (NADW). Subsequently, NADW cools the water, facilitating its southward transport. The model of Toggweiler & Bjornsson (2000) shows that the DP opening thus might have led to a cooling of the air and oceans around Antarctica of around 3°C. The water in the SH takes up the solar heat, which is then transported northwards where it is released, consequently warming up the NH by the equivalent amount the SH was cooled (Toggweiler and Bjornsson, 2000).

Lagabrielle et al. (2009) also discuss the influence of the proto-ACC on the formation/strength of Northern Component Water (NCW, later turns into NADW), which brings water from the NH to the Southern Ocean. Exactly when the formation of NCW began is unclear, but around 34 Ma the North Atlantic deepened rapidly due to its separation from Greenland in response to the Iceland mantle plume collapse, and significant deep-water production started in the NH (Lagabrielle et al., 2009; Via and

Thomas, 2006). Hence, along with tectonic changes in the North Atlantic region, the proto-ACC contributed to the inception of NCW/NADW and modulated its strength.

In the Eocene the SOGs were not open to deep ocean circulation. Rather, shallow ocean connections south of 60°S allowed for a westward Antarctic Counter Current (e.g., Bijl et al., 2013; Houben et al., 2019). Although SOGs progressively opened in the Oligocene (Stickley et al., 2004), oceanographic changes associated with that were restricted to the Southern Ocean (Houben et al., 2019; Scher and Martin, 2008), and there was little effect on the Southern Ocean oceanography for the remainder of the Oligocene (Evangelinos et al., 2020; Hill et al., 2013; Hoem et al., 2021; Wright et al., 2018). Only in the late Oligocene, Southern Ocean latitudinal SST gradients increased and perhaps the ACC strengthened, due to deep opening of Drake Passage (Hoem et al., 2022), although the ACC weakened again during the Miocene Climatic Optimum (Evangelinos et al., 2022; Sangiorgi et al., 2018).

3.3 Atmospheric pCO_2

Only a few records of atmospheric pCO_2 cover the Oligocene entirely. Most are focused on the EOT and the OMT, or are of low resolution. Trends are quite inconsistent between records and proxies (The Cenozoic CO2 Proxy Integration Project (CenCO2PIP) Consortium, 2023). The available records for the Oligocene are based on higher plant leaf gas exchange, phytoplankton ^{13}C-fractionation, and foraminifer boron isotope ratios (Fig. 1). Pagani et al. (2005) were the first to produce a pCO_2 record for the Oligocene using ^{13}C-fractionation of di-unsaturated alkenones extracted from various Deep Sea Drilling Program (DSDP) and Ocean Drilling Program (ODP) sediments. They recorded decreasing pCO_2 throughout the Oligocene from ~1500 ppm at the EOT to modern levels by the late Oligocene. Pagani et al. (2011) evaluated regional differences in pCO_2 and pCO_2 trends over the EOT by contrasting alkenone carbon isotope values from six DSDP and ODP Sites. The estimated pCO_2 values yielded highly variable results among the different sites showing a general atmospheric pCO_2 decline from around 1200 to around 600 ppm throughout the Oligocene, with pCO_2 decreasing around 40% at the EOT. Zhang et al. (2013) critically evaluated confounding factors of the alkenone pCO_2 proxy and excluded data from several locations, arriving at a continuous CO_2 record covering the past 40 Ma based on di-unsaturated alkenone ^{13}C-fractionation at ODP Site 925 in the western tropical Atlantic Ocean. The general findings of Zhang et al. (2013) agreed with the pCO_2 trends reported in Pagani et al. (2005, 2011) but showed pCO_2 values to decrease from ~1000 ppm at the EOT to ~400 ppm in the late Oligocene. Lastly, Witkowski et al. (2018) compiled the longest consecutive pCO_2 record of the past ~100 Ma, solely based on phytane ^{13}C-fractionation from marine sediment and oil samples. Their results concur with the findings of Zhang et al. (2013), showing pCO_2 ranges from ~600–1000 ppm throughout the Oligocene with a decreasing trend from the EOT towards the OMT (Fig. 1). Both Roth-Nebelsick et al. (2014) and Moraweck et al. (2019) used fossil leaf stomata to reconstruct Oligocene atmospheric pCO_2 levels. Oligocene fossil leaves of *Platanus neptuni* from various sites in Saxony (Germany) suggest lower pCO_2 levels than the alkenone-based results with a modelled range of ~400–600 ppm for the Oligocene (Roth-Nebelsick et al., 2014). Moraweck et al. (2019) reconstructed pCO_2 from the middle Eocene to the Oligocene using *P. neptuni* and *Rhodomyrtophyllum*

reticulosum leaves from 7 central European sites. They found a similar pCO_2 range as Roth-Nebelsick et al. (2014) with values also varying between ~400–600 ppm in the Oligocene. Greenop et al. (2019) created the only available boron isotope-based pCO_2 record, however they only focus on the OMT. While Greenop et al. (2019) did not find a strong decreasing trend over the OMT, they generally found low, stable values ranging from around 220 to 350 ppm, which increased to around 400 ppm after the OMT.

While there is a lot of variability between Oligocene pCO_2 records, with plant and boron data showing relatively stable pCO_2 levels, most other records suggest a steady decline of atmospheric pCO_2 towards the Miocene (The Cenozoic CO2 Proxy Integration Project (CenCO2PIP) Consortium, 2023).

4. Climate Proxy data

We compiled marine and terrestrial climate proxy data to assess long-term trends and variability in climate across the Oligocene. For sea surface temperatures, we have added recently published records to the compilation of O'Brien et al. (2020). To assess terrestrial climate, we compiled published records of fossil plant remains, notably pollen, spores, and macro-remains (appendix Table A1). Where the fossil plant remains had been assigned taxonomic affinities, the nearest living relatives (NLR) were determined and used as input for NLR-based probability density modeling, following the methodology of Willard et al. (2019) and Reichgelt et al. (2023), to assess terrestrial paleoclimate. We adopt the age determination from the original sources (appendix Table A1), corrected for the GTS 2020 stage boundaries (Gradstein, 2020), where absolute age determination is unavailable an average age was taken. Based on the distribution of the NLR for each fossil species, the probability of plant co-existence in an assemblage is calculated for 60,000 combinations of mean annual temperature (MAT), winter mean temperatures (WinT), mean annual precipitation (MAP) and driest month precipitation (DMP), as plant species distributions are sensitive to these variables and significant differences exist in the analyzed plant groups for these variables (see Supplementary Data). Up to 20 different plant taxa were compared at a time and where there were more than 20 taxa, sets of 10 were randomly chosen to maximize data variability. We report the highest probability climate combination, and the uncertainty range is based on those climatic combinations with a probability of ≥2.5% the maximum probability combination. We found 28 vegetation reconstructions of sufficient quality to assess paleoclimate using the NLR method (see appendix Table A1). The results can be assigned several potential quality "flags" based on diversity, depositional environment, and taxonomical assignments. First, low convergence of multiple simulations of the same flora may suggest that the climate niche of one or multiple taxa has changed since the Oligocene (Reichgelt et al., 2023). Additionally, some floras had fewer than 20 taxa recorded, for which convergence could not be tested. Second, microfloras (pollen and spores) likely include upland or even extra-basinal input and are therefore less indicative of local climatic conditions than macrofloras (leaves, fruits, flowers) (Reichgelt et al., 2023). Third and finally, some paleobotanical studies assign fossils to parataxa based on limited anatomical evidence, or using literature that is inappropriate for the study region. The majority of the data derives from NH mid-latitudes, a handful from SH mid-latitudes and two datasets from the tropical realm. The absence of high latitude data may be partly due

to the lack of vegetation owing to cool conditions. However, there are pollen assemblages in sediments from the Antarctic margin (e.g., Askin & Raine, 2000; Prebble et al., 2005; Raine & Askin, 2001), but to our knowledge no quantitative data suitable for our NLR method has been generated for any high-latitude site.

4.1 Temperature

4.1.1 Continental Mean Annual Temperature (MAT)

The data produced by the NLR allows for a first assessment of the general Oligocene meridional temperature gradient on land. Unfortunately, the data are too sparse to assess trends or variability at any location, on any time scale (Fig. 3). Although the sparsity of data from low and mid-latitude datasets limits our view on global gradients, the mid-latitude data can be compared to the modern and model simulations of the Oligocene, as well as to reconstructed Eocene and Miocene gradients.

The two low latitude data points suggest MATs of around 25°C (±1.5 °C). At first sight, Oligocene low latitude MATs were, on average, similar to modern MAT for the same latitudes. However, the NLR method is based on modern distributions and therefore reconstructed temperatures cannot exceed the global temperature maximum. Palaeobotanical temperature reconstructions from the tropics are susceptible to this problem and should therefore be considered minimum estimates. Most mid-latitude MAT reconstructions in both the Northern and SH are between 12 and 17 °C, with an average error of ±2.9°C (Fig. 3). Mid-latitude MAT, particularly in the SH, during the Oligocene are generally higher (up to 16°C) than modern temperatures. We did not encounter suitable data for high-latitude regions.

The reconstructed winter temperatures (WinT) range from ~23°C in the lower latitudes to ~3°C in the highest latitude samples (~52°N). Temperatures around the equator reveal limited change in winter cooling (~1.8°C), while at higher latitudes the difference in temperature between WinT and MAT can be up to nearly 8°C. Compared to modern values, Oligocene WinT show the same trend as MAT, with similar values (possibly underestimations) around the equator and higher temperatures in the mid-latitudes (Fig. 3). With the present dataset, it seems that Oligocene seasonality was similar to the modern, with WinT of the higher latitudes showing an up to ~12°C difference compared to the MAT, thus reflecting a high temperature change between MAT and Winter temperatures. Just as in the modern, Oligocene WinT had a large range at higher latitudes, with temperatures varying between ~5 – 15°C, whereas WinT of lower latitudes barely show any temperature difference (Fig 3).

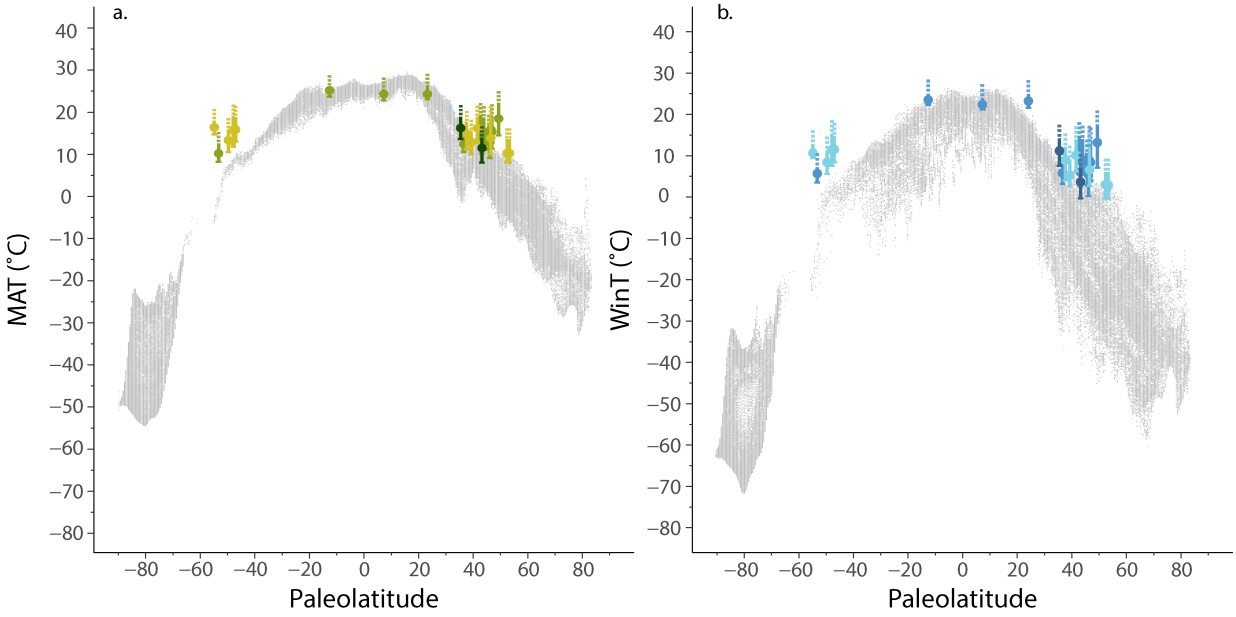

Figure 3: a. Mean annual temperature (MAT) plot over paleolatitudes, in grey: Pre-industrial (1900) MAT from Matsuura & Willmott, (2018); b. Winter Temperature (WinT) plot over paleolatitudes, in grey: Pre-industrial (1900) WinT from Matsuura & Willmott, (2018). Darker colours represent a higher analytical certainty of the used site, data with low reliability were excluded (see appendix Table A1).

4.1.2 Sea Surface Temperature

SSTs from three different proxies ($U^{k'}_{37}$, TEX_{86} and biogenic calcite $\delta^{18}O$) were compiled for the low-, mid-, and high latitudes of the Oligocene (Fig. 4). The alkenone-based SST reconstruction ($U^{k'}_{37}$), relies on the temperature dependence of di- and tri-C_{37} ketones (Prahl and Wakeham, 1987). At $U^{k'}_{37}$ values of >0.9 (at SSTs >27 °C) the proportion of the tri-unsaturated C_{37} alkenone becomes very low — virtually absent and/or undetectable, setting an upper limit for the application of this proxy (Tierney and Tingley, 2018). In addition, the low proportion of this alkenone introduces analytical uncertainties that cause noise. Consequently, we consider all $U^{k'}_{37}$ values >0.9 to represent SSTs at or above 27 °C. Following the recommendations by Hollis et al. (2019), we use the calibration of Müller et al. (1998, see appendix Table A2).

The TEX_{86} palaeothermometer is based on the temperature-sensitivity of marine thaumarchaeotal membrane lipid (isoprenoidal glycerol dialkyl glycerol tetraether (isoGDGT) distributions (Schouten et al., 2002). The proportion of GDGTs containing a greater number of cyclopentane rings increases with higher temperatures, and can thus be used to calculate SSTs using a modern surface sediment calibration (Wuchter et al., 2004). Discussion remains on how TEX_{86} should be calibrated to represent seawater temperatures. The surface sediment calibration dataset shows virtually no response to temperature below 15 °C and it is debated if the response at the high-temperature end of the modern ocean — analogous to warmer climates in

the past — can be assumed to be linear (e.g., O'Brien et al., 2017; Tierney & Tingley, 2014) or decreases exponentially (e.g., Cramwinckel et al., 2018; Kim et al., 2010). Moreover, isoGDGTs are barely produced in the mixed layer — they peak at ~50–200 m depth, and sometimes somewhat deeper (e.g., Hurley et al., 2018; van der Weijst et al., 2022). Most calibrations include surface ocean temperatures in their calibration dataset, leading to an overestimation of the proxy slope (Ho and Laepple, 2016). As the Oligocene was most likely warmer than today, we therefore prefer a conservative approach to assess SST, using an exponential calibration that has a drop in proxy-response at higher temperatures. Even though it is associated with regression dilution (Tierney and Tingley, 2014), we use the TEX_{86}^{H} of Kim et al. (2010, see appendix Table A2) to assess SST rather than a linear model, for reasons outlined in Fokkema et al. (in press). Linear models produce much higher SSTs in the Oligocene TEX_{86} range (Hollis et al., 2019). Moreover, any SST calibration assumes a similar relationship between surface temperature and the isoGDGT export zone in both modern and ancient oceans. Given the above uncertainties, it should be noted that absolute TEX_{86}-derived SST estimates come with large uncertainties.

Planktic foraminifer oxygen isotope ratios were also used to estimate Oligocene SSTs. This method is based on the direct correlation between the temperature dependent fractionation of the oxygen isotopes ^{16}O and ^{18}O into biogenic calcite of foraminifera (Shackleton, 1974). Here, the calibration of Kim & O'Neil (1997) is used because it is based on inorganic calcite precipitated at temperatures between 10 and 40 °C and produces reliable results for foraminifera (Hollis et al., 2019). Foraminiferal calcite production has been found to decrease with increasing pH levels (Zeebe et al., 1999; Spero et al., 1997). The calibration of Kim & O'Neil (1997), may overestimate temperatures by up to 1.5 °C, due to algal photosymbionts which modify the pH of the calcifying microenvironment (Spero and Williams, 1988). Although, applying a direct correction is not recommended (Hollis et al., 2019) due large uncertainties between symbiont activity levels, the influence of changing pH on SST reconstructions has to be considered.

Most available Oligocene SST data are from the mid-paleolatitudes; records for the low- and high latitudes, especially the NH, are scarce. Moreover, most records have low temporal resolution or cover only specific segments of the Oligocene (notably the EOT and OMT). The high latitude SSTs vary from 9.8 to 25.1 °C. It is worth noting that these records are restricted to latitudes no higher than 67°N and 68°S. SST estimates from mid-latitude locations have the largest temperature range, 6.0–32.1 °C, while SST estimates from low latitude sites span a narrower temperature range, 23.7–34.4 °C. The mid latitude SSTs show a slight increase (1–2 °C) between 34 Ma and ~27 Ma, followed by a small decrease of 1–2 °C towards 23 Ma (Fig. 4). However, overall, there is a remarkable absence of long-term trends in these SST records.

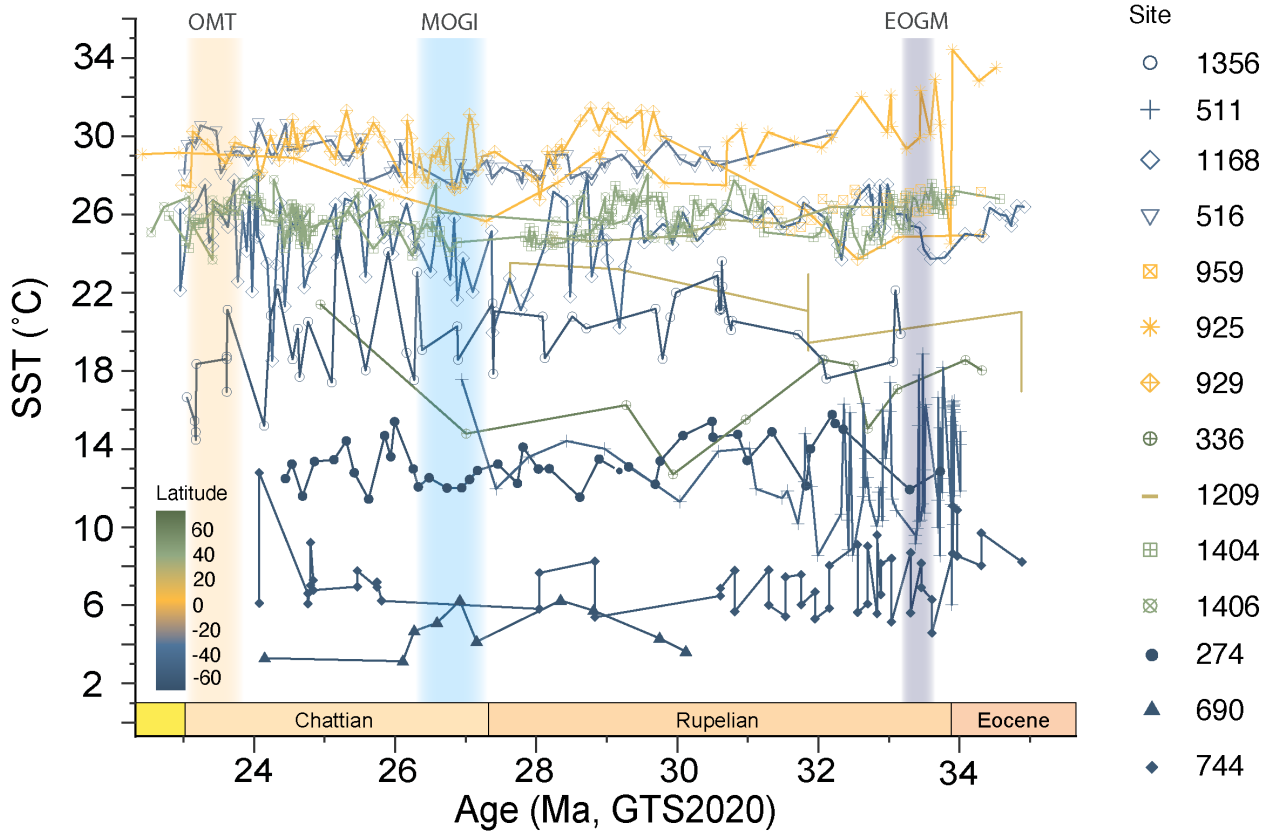

Figure 4: SST compilation for the Oligocene (The Cenozoic CO2 Proxy Integration Project (CenCO2PIP) Consortium, 2023). A linear interpolation was used between datapoints. Blue sites: SH high latitude sites; yellow sites: low latitude sites; green sites: NH high latitude sites. See Fig. 2 for site locations and appendix Table A3 for references.

To assess long-term changes in temperature and meridional temperature gradients, we analyze data from three time slices: 33.7–33.2 Ma, 27.3–26.3 Ma, and 23.9–23 Ma, corresponding to the EOGM, MOGI, and OMT, which are averaged for an age of 33.4 Ma, 26.8 Ma, and 23.4 Ma, respectively. When SSTs are corrected for paleolatitude (see appendix Table A3) Oligocene SSTs are closer to late Eocene (~38 Ma) than to modern values (Fig. 5). This is especially apparent in the Southern Ocean where Oligocene SSTs are up to 10 °C warmer than modern. The high latitudes of the NH are challenging to assess due to data scarcity. However, the data available indicate that Oligocene SSTs were ~2 °C colder than Eocene SSTs but still ~4 °C warmer than modern. In contrast, low latitude SST reconstructions show minimal differences, yielding similar temperature estimates for both the Oligocene and the Eocene. This leads to a flattened temperature gradient during the Oligocene between around 40°S and 40°N, where SSTs seem to be nearly the same.

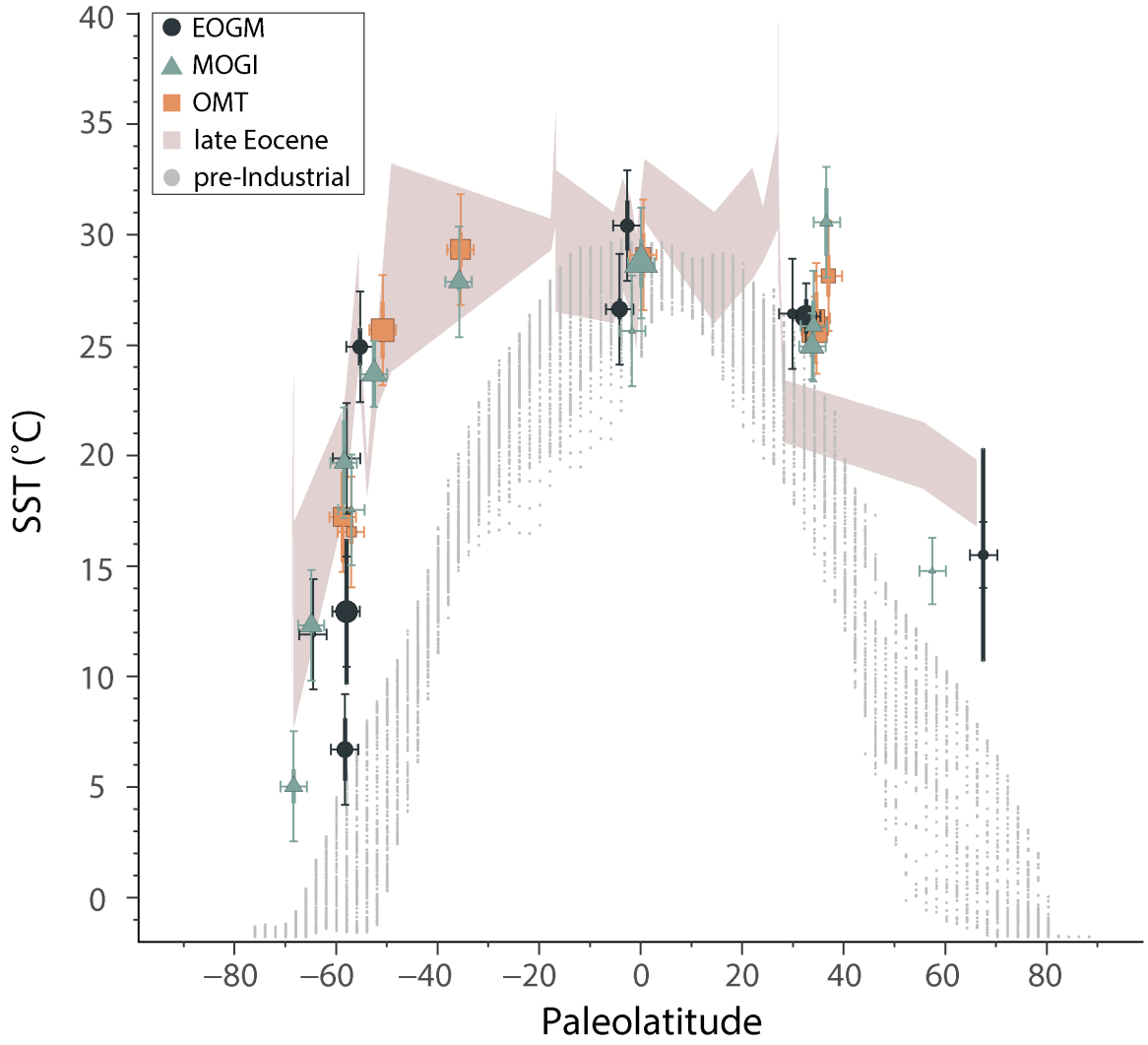

Figure 5: Sea surface temperatures (SSTs) over paleolatitudes for 33.4 Ma (EOGM, black dots), 26.8 Ma (MOGI, blue triangles), 23.4 Ma (OMT, orange squares). Brown shaded area: Baatsen et al., (2020) SST record for the late Eocene (38 Ma). Grey area: Pre-industrial (1900) SST over latitude (Huang et al., 2015). Thick vertical error bars show the SST standard deviation, thin vertical error bars represent the calibration error for each proxy. Larger symbols represent a higher data resolution, with larger symbols representing more data used and smaller points where less data was available. See appendix Table A3 for data referral and references used.

4.2 Precipitation

Mean annual precipitation (MAP) and driest month precipitation (DMP) were derived using the NLR approach (Table 1). The reconstructed MAP shows a range from ~850 mm/yr to 1750 mm/yr. The SH mid-latitudes show a generally higher MAP

(~1200–1750 mm/yr) for the Oligocene compared to the NH (~850–1650 mm/yr). This differs from modern MAP values, where there is not a big discrepancy between SH and NH MAP. Generally, the Oligocene MAP values are higher than modern values, especially at mid-latitudes. The few datapoints in the tropics suggest similar to modern MAP. The values for the driest month range from ~10 mm/yr to 85 mm/yr with generally lower values around the equator and the NH (~10–45 mm/yr) and higher DMP on the SH (~20–85 mm/yr). The DMP values around the equator are generally lower compared to modern values. In contrast to the Oligocene, the modern SH DMP are on average lower than NH DMP values.

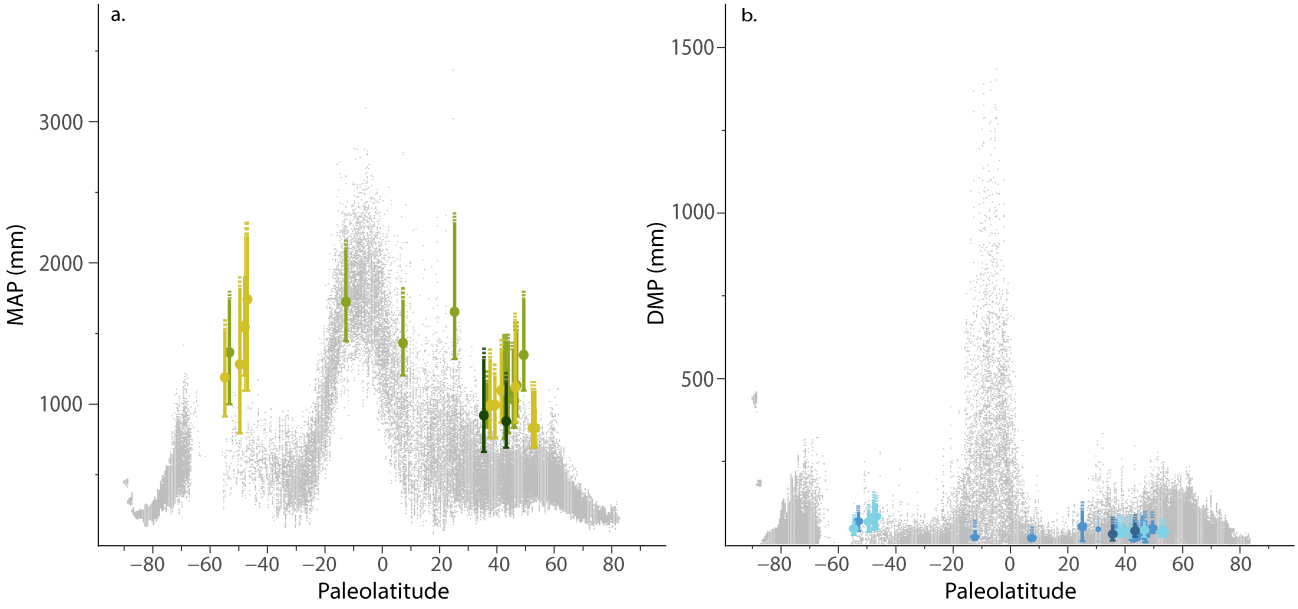

Figure 6: a. Mean annual precipitation (MAP) plot over paleolatitudes in mm per year, in grey: Pre-industrial (1900) MAP via Matsuura & Willmott, (2018); b. Driest month precipitation (DMP) plot over paleolatitudes in mm per year, in grey: Pre-industrial (1900) DMP via Matsuura & Willmott, (2018). Darker colours represent a higher analytical certainty of the used site, data with low reliability was excluded (see appendix Table A1).

4.3 Data–Model Comparisons

The compiled surface temperature and precipitation data was regionally compared against the results from paleoclimate model simulations (Figs. 7 and 8). Following the methodology described by O'Brien et al. (2020), two sets of modelling experiments were used: one from the NCAR Community Earth System Model version 1.0 (CESM1.0) and the other from the UK Hadley Centre Coupled Model version 3 (HadCM3L). The early and middle Oligocene simulations were performed using a x3° nominal ocean and the T31 atmospheric resolution with varying glaciation conditions and pCO_2 of 560 and 1120ppm. The late Oligocene simulation is using a x1° nominal ocean and 2° atmospheric resolution with a pCO_2 of 400ppm. We compare data and simulations for three time slices (a. early Oligocene, 33.9–33.0 Ma; b. mid Oligocene, 33.0–26.5 Ma; c. late Oligocene,

25.0–23.5 Ma, Fig. 7). For each time slice, the model ensemble mean is used to compare with the data, and the modelling details of the ensemble members are found in the Methods and Supporting Information Table S1 of O'Brien et al. (2020). The model annual mean values are derived from the nearest grid point to the study site.

4.3.1 Temperature proxy to model comparison

Despite utilizing two very distinct models with different boundary conditions, the temperature discrepancy between the model and data is similar. The comparison of sea and land temperatures of all three time slices, show that the mid and high latitude proxy data generally suggests warmer local conditions than simulations predict (Fig. 7). For all investigated time slices, that discrepancy is largest in the North Atlantic and southwest Pacific. Additionally, for every time slice, the tropics seem to be warmer in model simulations than what local proxy data find, with the most extreme discrepancies in continental southeastern Asia. For the early and middle Oligocene, there is a difference between the modelled higher latitudes and measured data. In both the early and middle Oligocene, the higher latitudes seem to be a lot warmer (up to 20°C) in the proxy data than what the models predict. The lower latitudes on the other hand, for both the early and middle Oligocene, seem somewhat colder (around 5°C) than what models predict. In the early Oligocene, North America generally shows a similar temperature range as the European sites, with proxy data indicating warmer conditions compared to the model. This shifts in the middle Oligocene, where most of the recorded North American sites are colder than what the models predict. The late Oligocene seems to have a similar offset in the SH high latitudes, with reconstructed temperatures being up to nearly 20°C higher than the model results. Due to the lack of proxy data in the NH high latitudes and the tropics, temperature differences between models and records cannot be determined for the late Oligocene.

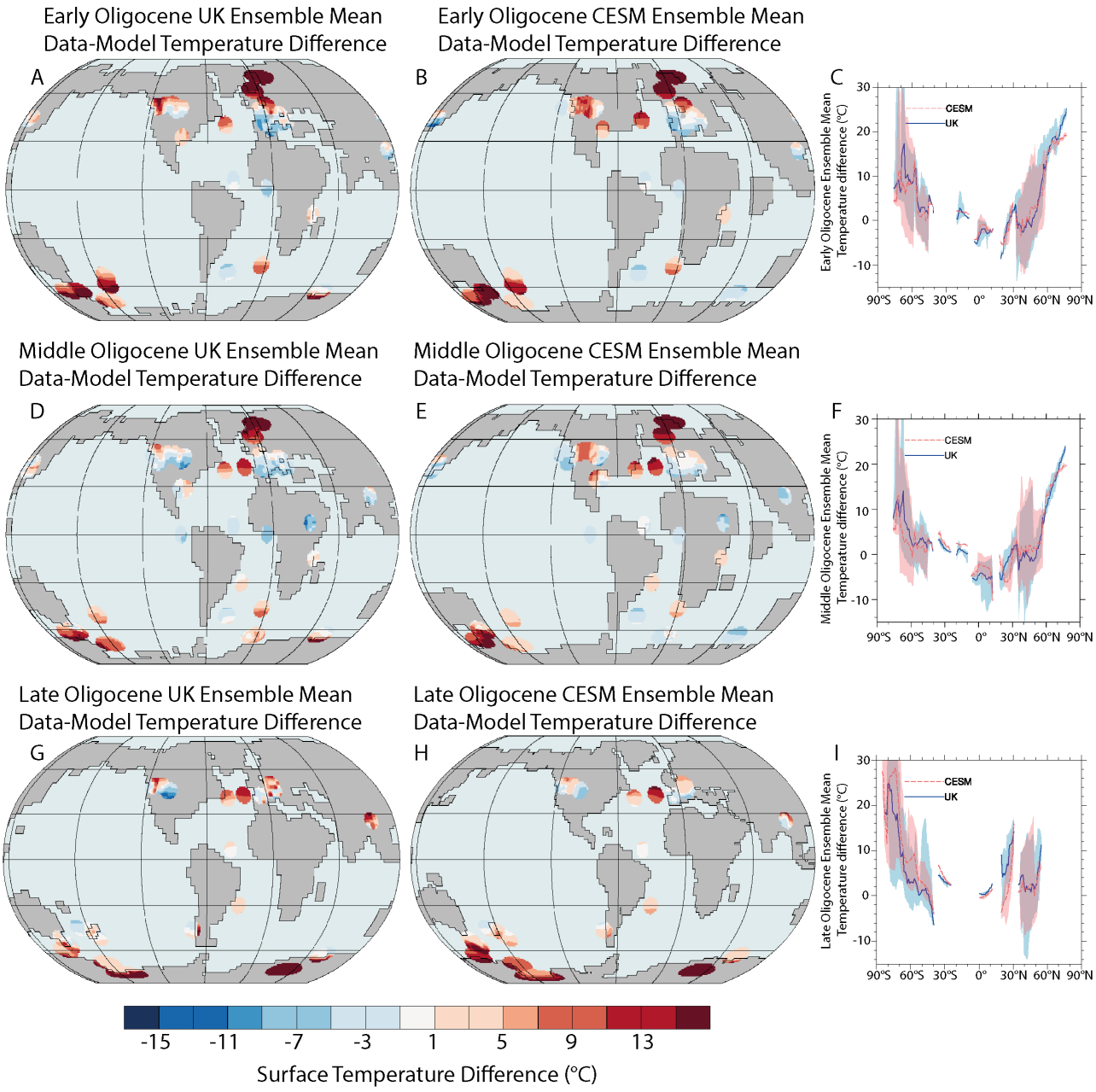

Figure 7: Oligocene temperature data to model comparisons. All proxy data were compared to ensemble means from HadCM3L (UK) and CESM models. (A–I) Sea surface and Land temperature data-model comparisons for three Oligocene time slices. Data-model temperature difference data are displayed both spatially (A, B, D, E, G, H) and as zonal means (C, F, I). Temperature difference data in A, B, D, E, G, H are calculated as pointwise differences between the proxy mean value and the model annual mean. The pink and blue ribbons in C, F and I represent the maximum and minimum differences associated with the zonal means. All proxy data are shown in appendix Table A4.

4.3.2 Precipitation proxy to model comparison

Comparison of precipitation proxy data to modelled simulations shows, that for all three simulated times, models mostly slightly underestimate the daily precipitation on a global scale (Fig. 8). In particular, the SH mid to lower latitudes seem to be much drier in the models that what the proxy data suggest. For the early Oligocene only NH tropical and NH mid latitude data are available, indicating a slightly wetter (300 – 400mm/yr) climate in Europe, whereas eastern Asia and western North America appear to be drier (300 – 900mm/yr) than model predictions. Due to limited proxy data, we cannot make definitive statements about the early Oligocene in North America and eastern Asia. In the middle Oligocene, although more proxy data is available compared to the early Oligocene, the patterns are similar. Compared to the model results, the proxy data suggest wetter climates (300 – 400mm/yr) in Europe and eastern Asia (600 – 900mm/yr) and somewhat drier conditions (300 – 900mm/yr) in North America. In both the middle and late Oligocene, model simulations appear to underestimate precipitation in SH mid- to high latitudes (300 – 900mm/yr) (Fig. 8). Similar to the early and mid-Oligocene, late Oligocene precipitation over central Europe and the region corresponding to today's Middle East also appear to be underestimated by models (300 – 900mm/yr), although precise quantifications cannot be made due to the lower proxy resolution.

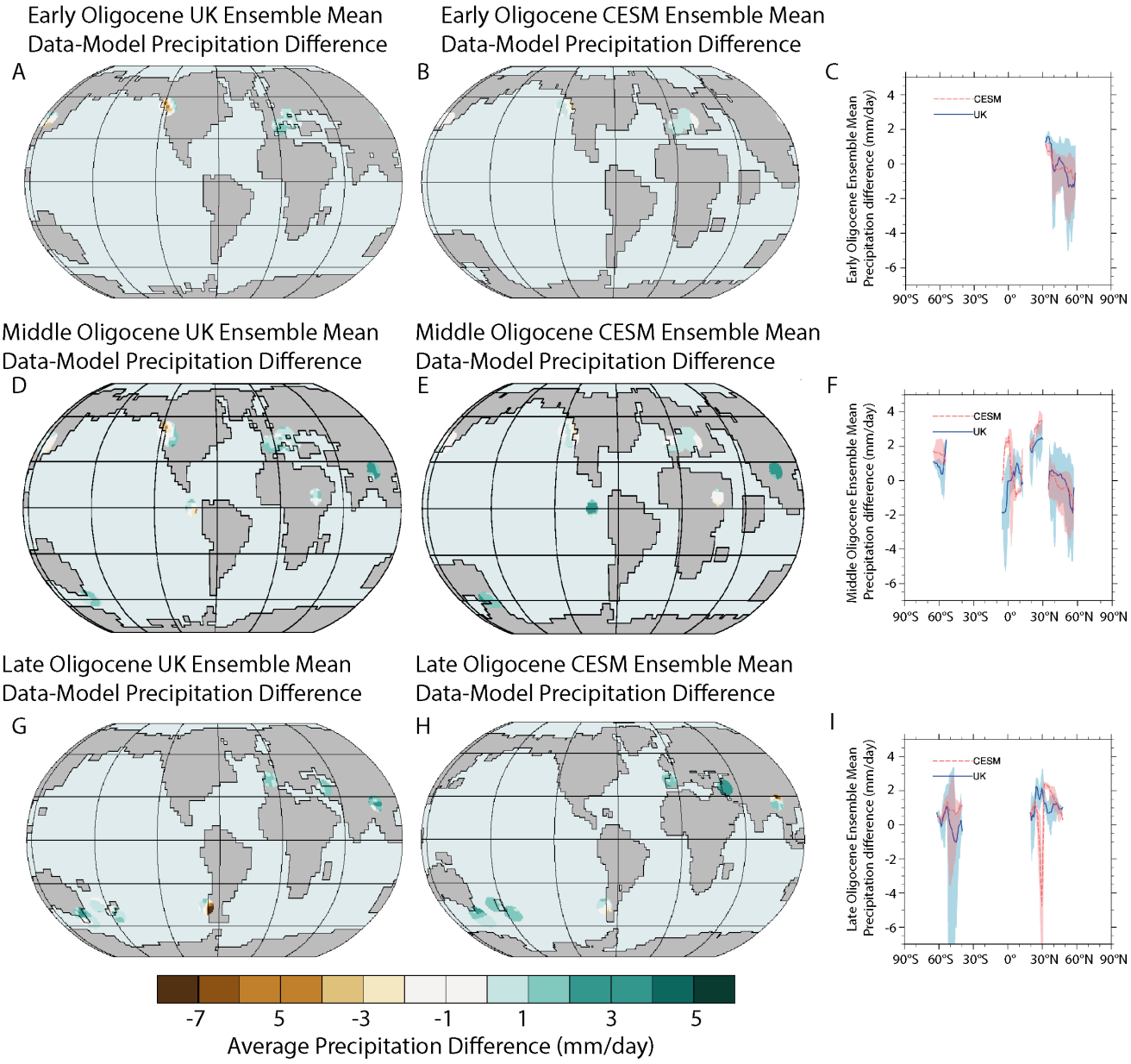

Figure 8: Oligocene precipitation data (mm/day) to model comparisons. All proxy data was compared to ensemble means from HadCM3L (UK) and CESM models. (A–I) Precipitation data–model comparisons for three Oligocene time slices. The data is both displayed in a spatial (A, B, D, E, G, H) and zonal mean (C, F, I) of the different precipitations. Differences in A, B, D, E, G and H are calculated as a pointwise difference between the proxy mean value and the model annual mean and then plotted as points of differences. The pink and blue ribbons in C, F and I represent the maximum and minimum differences associated with the zonal means. All proxy data are shown in appendix Table A5.

5. Discussion

5.1 Temperature trends and variability

Our compilation of data shows that not only were the Oligocene oceans warm (O'Brien et al., 2020), but also the sparsely available floral and faunal information from terrestrial settings show pronounced warmth (Fig. 3). On average, the data indicate that the Oligocene was slightly cooler than the Eocene, but much warmer than modern times (Figs 3, 5). Notably, the high latitudes were much warmer than modern. The current dataset suggests no or only modest tropical warming relative to the present, but it should be noted that this is based on few records and the expected ocean warm pools have not yet been sampled. Both sea surface and terrestrial temperature gradients between the tropics and SH midlatitudes were particularly small, which was previously recognized for the Eocene as well as for the Miocene (e.g., Baatsen et al., 2020; Burls et al., 2021; Hollis et al., 2019; Lunt et al., 2021). For both Eocene and Oligocene SSTs, this is mainly the result of very high proxy values in the southwest Pacific and the Australo-Antarctic Gulf (Baatsen et al., 2020; O'Brien et al., 2020). The gradient is very steep beyond 50°S (Fig. 5) while the equator to pole temperature gradient in the NH is more gradual. This means that despite the presence of ice in Antarctica, the mid-latitudes of the SH seem to be especially warm in the Oligocene.

Single-site high resolution benthic foraminifer isotope data show a gradual decrease in $\delta^{18}O$ values across the late Oligocene up to the onset of the OMT (Figure 1; (De Vleeschouwer et al., 2017; Liebrand et al., 2016; Pälike et al., 2006b). This suggests pronounced warming during the late Oligocene, termed Late Oligocene Warming. Regionally, this warming is supported by biogeographical information (De Man and Simaeys, 2004). Yet, the compiled temperature records show no consistent evidence for long-term warming throughout the mid to late Oligocene. Rather, they show relatively stable values, with only few records (e.g., ODP 925, 744) indicating cooling from the early- to mid-Oligocene, followed by long-term warming from the mid to late Oligocene (Fig. 4). This suggests that the decrease in $\delta^{18}O$ values may reflect regional warming at deep-water formation sites rather than global warming.

On the shorter term, there is strong variability within the temperature data – especially for the high- and mid-latitudes (Fig. 4). Currently the resolution of all temperature records is insufficient to assess if any of this variability corresponds to orbital cyclicity. Similar variability apparent in deep ocean benthic $\delta^{18}O$ records primarily reflects eccentricity signals on around 110 ka timescales (Pälike et al., 2006b; Westerhold et al., 2020). If the temperature variability is global in nature, its increasing amplitude towards higher latitudes would likely reflect a combination of climatic polar amplification (i.e., ice/snow albedo and humidity feedbacks) and/or oceanographic variability (i.e., fronts and upwelling). Yet, due to the low resolution and lack of temperature records in especially low latitudes and the NH, the nature of and mechanism behind the temperature variability remains uncertain.

When compared to model simulations (Fig. 7 and 8), it is evident that the models show significantly less polar amplification of warming relative to the present day than the proxy data. This is due to the extremely strong warming at higher latitudes and comparatively modest warming in the tropics in the proxy data, compared to the simulations. The dataset is limited as floral data might underestimate temperatures in warmer-than-modern tropical regions (e.g., Huber & Caballero, 2011). It should also

be noted that some of the SST data is based on TEX_{86}, which suffers from large uncertainties in absolute SST reconstructions (see section 4.1.2). However, plant based (NLR) and $U^{k'}_{37}$ derived temperatures show similar warming as those based on TEX_{86} in the high latitudes, corroborating strong polar amplification. In other parts, climate models are not able to fully reconstruct regional climate variations as closely as proxy data can, and thus probably underestimate regional variability, particularly on land (e.g., (Laepple et al., 2023). Additional high-quality SST data is necessary to fully evaluate tropical temperatures for the Oligocene.

Particularly the shallow gradient between the equator and ~40 ° N and S is difficult to reconcile with the simulations. Floral data and carbonate geochemical records support exceptional mid-to-high latitude warmth during the Eocene (e.g., Creech et al., 2010; Douglas et al., 2014; Willard et al., 2019) which seems to still be the case during the Oligocene. Collectively, the nature of the data might underestimate the latitudinal heat transfer for the Oligocene. Regardless, our findings agree with those of O'Brien et al. (2020), showing that most of the Oligocene was similar to the late Eocene greenhouse world. Like in the late Eocene (Baatsen et al., 2024), the recorded temperatures are difficult to reconcile with the formation and persistence of a large ice sheet on Antarctica. The model-data comparison highlights the ongoing challenges of fully understanding the complex nature of the Oligocene. Questions remain regarding the formation of ice in a world with a flattened meridional temperature gradient, when poles were much warmer than today and atmospheric CO_2 levels were high (e.g., Baatsen et al., 2020, 2024).

5.2 Precipitation

Surprisingly, the few MAP datapoints at low latitudes are similar to today (Fig. 6), whereas mid-latitude MAP is higher compared to pre-industrial values. DMP for the Oligocene low latitudes is especially low compared to preindustrial. The southern Hemisphere mid to high-latitude DMP (~100 mm/yr) is higher than pre-industrial records ($<100 mm/yr$), whereas the DMP for the Northern Hemisphere is lower (~50 mm/yr), which is more in line with the pre-industrial records (0 – 250 mm/yr). During periods that are globally warmer than today, the tropics and the mid-latitudinal zone of converging westerlies (30–60° latitude) would be expected to be wetter than today, while the subtropics would be expected to be drier (e.g., Pierrehumbert et al., 2002).This is consistent with MAP reconstructions, especially at >30° (Fig. 6a), whereas the data from lower latitudes is less clear, but that is largely due to a dearth of datapoints. Overall, Northern Hemisphere MAP is lower than that of the Southern Hemisphere. This may be due to the prevalence of Northern Hemisphere continental climate systems in the Oligocene (e.g., Sun et al., 2014). The Oligocene reconstructed MAP is somewhat lower than those of the Eocene (Cramwinckel et al., 2022). This drier climate compared to the Eocene is also seen in other terrestrial records (e.g., Couvreur et al., 2021; Dupont-Nivet et al., 2007; Jaramillo et al., 2006; Kohn et al., 2015; Ma et al., 2012; Salard-Cheboldaeff, 1979; Sun et al., 2014), which suggests the expansion of arid regions and reduction of rainforests during the Oligocene.

In addition, comparisons to modelled data shows that the models underestimate, particularly higher latitude, precipitation levels from 300 up to over 900mm/yr. Paleoclimate models homogenize meso- and microclimates due to the large grid size which leads to an averaged topography and thus less spatial precipitation variability. Proxy data, on the other hand, may

experience a bias to wetter environments, as there is more plant data available where wetter climates persisted, including those in meso- or microclimates that were unrepresentative of the macroclimate, such as a riparian environment. Similar to temperature (section 6.1), our understanding of global Oligocene precipitation relies on a limited dataset, mainly sampling Europe (Fig. 2) and therefore a first-order goal to a more comprehensive understanding of Oligocene paleoclimates would be generating more terrestrial data from other continents, particularly from high-latitude regions.

6. Conclusions and outlook for future work

While the paleogeography of the Oligocene differs from today, it still poses a useful analogue to a projected future unipolar climate state. It is becoming more and more clear that the Oligocene icehouse was in fact warmer than previously thought, particularly in mid and high latitudes. However, the present dataset suggests that the tropical band was not much warmer than today. This is contrary to model simulations, which predict higher-than-modern tropical regions for the Oligocene and thereby most likely underestimate polar amplification and subsequent equator-to-pole heat distribution. From this perspective, the Oligocene also contrasts with reconstructions of tropical temperatures for the Miocene and Eocene (e.g., Steinthorsdottir et al., 2021; Hollis et al., 2019). Consequently, tropical climates during the Oligocene require further investigation and in addition to the present dataset, which is notably based on biomarkers, proxies based on well-preserved biogenic calcite derived from surface oceans are crucial. In contrast to tropical regions, proxy records at mid and high-latitude regions suggest extreme warmth, as also noted for the Miocene and Eocene epochs (e.g., Steinthorsdottir et al., 2021; Hollis et al., 2019). The low temperature gradients indicated by our data remain a model-data mismatch that requires solving due to its implications for the processes governing polar amplification of greenhouse gas-driven warming and the magnitude thereof.

The limited vegetation data available support higher precipitation in mid-latitude regions during the Oligocene, as predicted by theory and model simulations. However, the continental dataset is limited, and more data is required particularly for the tropical band and the high latitudes to test for tropical hydrology and high latitude winter temperatures, respectively.

Our temperature compilation does not show systematic long-term changes in temperature during the Oligocene. With the typically low resolution of the available long-term records, temperatures remained approximately stable. This is at odds with the long-term trends in the benthic foraminifera $\delta^{18}O$ record, which shows signs of early Oligocene cooling and late Oligocene warming, albeit low in magnitude. Higher-resolution SST reconstructions at multiple locations are required to fully evaluate if those trends are absent on Earth's surface. Moreover, the apparent absence of long-term trends in SST and the nature of the minor trends in benthic foraminifera $\delta^{18}O$ are both inconsistent with the recorded long-term drop in atmospheric pCO_2. This is a truly interesting conundrum and one that requires long-term high resolution pCO_2 reconstructions to fully evaluate. Although the benthic foraminifera $\delta^{18}O$ records have identified the orbital-scale dynamics of deep ocean temperature and/or continental ice volume in detail, orbital-scale climate variability of the Oligocene on the surface is poorly constrained. SST records resolving orbital-scale variability are required to ultimately characterize the nature of global mean surface temperature

variability as well as the magnitude of polar amplification, its dependence on atmospheric pCO_2, and its relation to global continental ice volume.

Finally, an outstanding question remains on the relation of climate variability and subsequent biotic change. There is ample micropaleontological evidence for a biotic response to orbital-scale temperature variability for the Oligocene (e.g., De Man and Simaeys, 2004; Śliwińska et al., 2010; Hoem et al., 2021; Fenero et al., 2013). The interplay of long-term climate stability and superimposed orbital scale variability provides a very interesting opportunity to investigate the systematic relation between such climate variability and biotic resilience. This requires long-term high resolution micropaleontological records but might ultimately result in much better-defined thresholds of massive regime shifts.

7. Appendix A

Locality	Average Age (Ma)	Latitude	Paleolatitude	Number of Taxa	Number of Simulations	Quality Flags	Min MAT (°C)	MAT (°C)	Max MAT (°C)	Min WinT (°C)	WinT (°C)	Max WinT (°C)	Min MinT (°C)	MinT (°C)	Max MinT (°C)	Min MAP (mm/yr)	MAP (mm/yr)	Max MAP (mm/yr)	Min DMP (mm/yr)	DMP (mm/yr)	Max DMP (mm/yr)	References
As Pontes basin	26.1 ±3.7	43.45	37.62	14	1	Taxa assignments dubious, one simulation, macrofloras	11.2	14.8	17.7	4.0	8.9	12.1	-0.8	1.9	7.0	759	1000	1318	20	38	63	Cabrera et al. 1995
Belen Fruit & Seed assemblage	29.25 ±0.75	-4.75	-12.62	17	1	Taxa assignments reliable, one simulation, macroflora	23.7	25.2	25.9	22.3	23.5	25.0	15.1	16.9	18.9	1445	1738	2089	11	20	40	Manchester et al. 2012
Berwick Quarry	25	-38.03	-47.02	33	10	Taxa assignments reliable, high convergence, macro- and microfloras	13.0	15.9	18.8	8.4	11.6	14.7	3.5	6.1	9.5	1096	1754	2188	44	78	120	Pole et al. 1993
Calau Beds	29.5 ±1.5	51.78	46.86	56	10	Taxa assignments reliable, medium convergence, macrofloras	11.3	15.4	19.2	3.9	8.4	13.7	-1.3	2.6	6.5	912	1143	1514	4	24	69	Mai 1998
Cervera (Rasqui quarry, Carulla quarry, Mas Claret, Briançó)	30.85 ±3.05	41.65	35.44	28	10	Taxa assignments reliable, high convergence, macroflora	13.6	16.3	18.9	7.6	11.2	14.2	1.7	5.5	8.8	661	955	1318	9	24	58	Tosal & Martín-Closas 2016
Cosy Dell	24.9 ±0.5	-46.15	-47.91	65	10	Taxa assignments reliable, medium convergence, microfloras	12.6	15.8	17.8	8.6	11.4	14.0	3.5	6.2	8.9	1202	1556	1905	48	74	115	Conran et al. 2014
Daxing'anling	31.15 ±2.75	45.86	52.40	24	10	Taxa assignments reliable, high convergence, microfloras	8.0	10.3	13.6	-0.4	3.0	6.0	-5.3	-1.5	1.5	692	843	1096	20	32	55	Ma et al. 2012
Daxing'anling 2		46.73	53.31																			
Guang River	27.23	12.60	7.24	19	1	Taxa assignments reliable, one simulation, macroflora	22.8	24.3	25.5	21.2	22.4	23.9	14.3	16.9	18.4	1202	1445	1738	8	14	29	Pan 2007
Haselbach Horizon	29.75 ±0.75	51.42	46.45	32	10	Taxa assignments reliable, medium convergence, macroflora	12.8	15.9	18.8	4.9	8.9	13.9	-0.2	3.3	7.5	871	1143	1585	15	33	55	Kunzmann & Walther 2012
Haynes Creek Flora	30	45.00	43.22	29	10	Taxa assignments reliable, high convergence, macroflora	8.0	11.5	13.9	-0.3	3.7	7.1	-5.4	-0.7	2.4	692	891	1148	20	37	63	Axelrod 1998
Hrazený hill	29.5 ±1.5	50.98	46.11	32	10	Taxa assignments reliable, low convergence, macroflora	9.1	12.9	16.2	0.2	5.4	9.0	-5.8	0.9	3.2	832	1038	1380	20	35	66	Kvaček et al. 2015
Kraskino Flora	30	42.71	49.33	31	10	Taxa assignments reliable, low convergence, macrofloras	14.5	18.5	22.2	7.1	13.2	17.6	1.9	6.4	11.4	1096	1361	1738	32	43	69	Pavlyutkin 2011
Lea River	31 ±1	-41.50	-53.28	10	1	Taxa assignments reliable, one simulation, macroflora	8.2	10.2	12.6	3.5	5.7	7.2	-1.0	1.3	3.5	1000	1380	1738	38	63	95	Paull & Hill 2010
Maikop Group	25	40.55	39.29	30	10	taxa assignments reliable, high convergence, microfloras	10.1	12.8	15.6	2.6	5.3	9.1	-1.9	0.8	3.3	759	1005	1202	23	36	58	Popov et al. 2008
Makum Coal Field	26.2 ±3.2	27.25	25.46	23	10	Taxa assignments dubious, high convergence, macroflora	23.1	24.3	26.4	21.6	23.2	24.9	16.4	18.5	20.7	1318	1667	2291	7	45	100	Awasthi & Mehrotra 1995
Monpeelyata deposit	23.3 ±0.9	-41.83	-49.68	43	10	Taxa assignments reliable, medium convergence, microfloras	10.5	13.3	15.9	5.6	8.4	11.3	0.2	3.2	6.5	794	1294	1820	35	63	100	Macphail et al. 1991
Newvale Mine	24.1 ±1.1	-46.14	-47.91	99	10	Taxa assignments reliable, low convergence, microfloras	11.8	15.7	19.1	7.5	11.4	15.3	2.5	6.3	10.9	1096	1556	2188	42	84	132	Ferguson et al. 2010
Paleogene basin	30.45 ±3.45	46.35	41.54	26	10	Taxa assignments reliable, low convergence, macrofloras	12.8	16.2	18.9	6.2	10.2	13.9	1.1	4.0	7.6	871	1107	1380	17	38	63	Erdei et al. 2012
Pitch-Pinnacle flora	30.95 ±1.95	39.12	36.56	17	1	Taxa assignments reliable, one simulation, macroflora	10.6	12.4	13.9	3.2	5.8	7.8	-1.4	0.8	2.4	832	1047	1148	26	38	52	Gregory & McIntosh 1996
Rauenberg	29.5 ±2.5	49.27	43.97	35	10	Taxa assignments reliable, medium convergence, macroflora	12.3	15.3	18.7	5.6	9.0	14.0	0.9	4.1	8.1	794	1091	1445	12	30	55	Kovar-Eder 2016
Roudníky area	31.95 ±1.95	50.65	45.75	33	10	Taxa assignments reliable, medium convergence, macrofloras	11.2	14.1	16.8	2.8	6.9	10.6	-2.6	1.7	4.7	832	1102	1380	20	35	58	Kvaček et al. 2014
San Julian Fm	24	-49.16	-54.85	18	1	Taxa assignments reliable, one simulation, microfloras	14.7	16.4	18	9.4	10.7	12.8	2.5	4.1	6.9	912	1202	1514	26	42	69	Palazzesi & Barreda 2007
Suletice-Berand	27.5 ±1.5	50.61	45.89	17	1	Taxa assignments reliable, one simulation, macroflora	12.6	14.5	16.1	6.0	8.7	10.3	0.5	1.8	4.4	871	1096	1380	28	42	60	Kvaček & Walther 1995
Tard Clay1	32.9 ±0.9	47.50	42.73	12	1	Taxa assignments reliable, one simulation, macroflora	14.6	16.9	19.4	8.3	11.6	14.8	2.5	7.0	8.9	759	1000	1445	8	13	35	Kvacek et al. 2001
Tard Clay2		47.91	42.73																			
upper Ruby Basin	32.9 ±0.7	45.11	43.10	65	10	Taxa assignments reliable, medium convergence, macroflora	10.2	13.5	16.8	2.7	6.0	11.0	-2.8	1.3	5.4	794	1028	1318	18	34	58	Becker 1966
Weißelster	29.75 ±0.75	51.42	46.45	79	10	Taxa assignments reliable, low convergence, macrofloras	10.0	13.9	18.9	2.7	6.6	12.3	-1.7	1.5	5.7	871	1138	1585	20	39	66	Gastaldo et al. 1998

Table A1: Results of the nearest living relative (NLR) analysis, showing mean annual temperature (MAT), winter mean temperatures (WinT), mean annual precipitations (MAP) and driest month precipitation (DMP) and their respective minimum and maximum values.

SST Proxy	SST calibration details	References
U^{K}_{37}	$U^{k'}_{37}$ indices were converted to SST estimates using the global core-top calibration of Müller et al., 1998.	Müller PJ, Kirst G, Ruhland G, Von Storch I, & Rosell-Melé A (1998) Calibration of the alkenone paleotemperature index $U^{K'}_{37}$ based on core-tops from the eastern South Atlantic and the global ocean (60°N-60°S). *Geochimica et Cosmochimica Acta* 62(10):1757–1772.
TEX_{86}	TEX86 values were converted to SST using the global logarithmic TEXH86 calibration of Kim et al. (2010).	Kim, J.-H. et al. New indices and calibrations derived from the distribution of crenarchaeal isoprenoid tetraether lipids: implications for past sea surface temperature reconstructions. Geochim. Cosmochim. Acta 74, 4639–4654 (2010).
Δ_{47}	Δ47 SST estimates and sample age were taken directly from the original publications.	Douglas, P. M. J. *et al.* Pronounced zonal heterogeneity in Eocene southern high-latitude sea surface temperatures. *Proceedings of the National Academy of Sciences* **111**, 6582-6587 (2014). Evans, D. *et al.* Eocene greenhouse climate revealed by coupled clumped isotope-Mg/Ca thermometry. *Proceedings of the National Academy of Sciences* **115**, 1174–1179, doi:10.1073/pnas.1714744115 (2018). Petersen, S. & Schrag, D. Antarctic ice growth before and after the Eocene-Oligocene transition: New estimates from clumped isotope paleothermometry. *Paleoceanography and Paleoclimatology* **30**, 1305–1317, doi:10.1002/2014PA002769 (2015). Briard, J. et al. Seawater paleotemperature and paleosalinity evolution in neritic environments of the Mediterranean margin: insights from isotope analysis of bivalve shells. Palaeogeogr. Palaeoclimatol. Palaeoecol. 543, 109582 (2020).
$\delta^{18}O$ coccoliths	SST estimates are original published values for small coccoliths with a vital effect correction in Tremlin et al., 2016.	M. Tremblin, M. Hermoso, F. Minoletti, Equatorial heat accumulation as a long-term trigger of permanent Antarctic ice sheets during the Cenozoic. Proc. Natl. Acad. Sci. U.S.A. 113, 11782–11787 (2016).
$\delta^{18}O$ planktic foraminifera	Palaeotemperature estimates were generated using the calibration of Kim & O'Neil (1997).	Kim, S. T., & O'Neil, J. R. (1997). Equilibrium and nonequilibrium oxygen isotope effects in synthetic carbonates. *Geochimica et cosmochimica acta*, *61*(16), 3461-3475.

Table A2: Summary of the calibrations and references thereof used for the respective sea surface temperature (SST) proxies.

570

23.9 - 23.0 Ma

Site	Latitude	Longitude	Event	Average Age (Ma)	Proxy	Number of Data points	Paleolatitude	Lowest Latitude	Highest Latitude	Min Latitudinal error	Max Latitudinal error	Average SST (°C)	Standard deviation (°C)	Analytical error (°C)	Calibration error (°C)	References
269	-61.68	140.07	OMT	23.4	TEX86	2	-57.1	-59.73	-54.53	2.7	2.5	16.54	0.54	1.00	2.50	Evangelinos et al. 2020
1356	-63.31	136.00	OMT	23.4	TEX86	9	-58.7	-61.38	-56.18	2.6	2.6	17.23	2.04	1.00	2.50	Hartman et al. 2018
1168	-42.61	144.41	OMT	23.4	TEX86, UK37	14	-50.9	-53.54	-48.33	2.7	2.5	25.68	1.29	1.00	2.50	Guitian & Stoll 2021, Hoem et al. 2022
1404	40.01	-51.81	OMT	23.4	UK37	18	34.2	31.69	36.89	2.5	2.7	25.70	0.58	0.30	1.50	Liu et al. 2018
1406	40.35	-51.65	OMT	23.4	UK37, TEX86	7	34.5	32.01	37.22	2.5	2.7	26.21	1.17	1.00	2.50	Guitian et al. 2019
608	42.84	-23.09	OMT	23.4	TEX86	4	36.9	34.38	39.59	2.5	2.7	28.14	0.93	1.00	2.50	Super et al. 2018
929	5.98	-43.74	OMT	23.4	TEX86	5	0.4	-2.16	3.05	2.6	2.6	29.08	1.00	1.00	2.50	O'Brien et al. 2020, Liu et al. 2009
516	-30.28	-35.29	OMT	23.4	TEX86	10	-35.5	-38.20	-33.00	2.7	2.5	29.33	0.77	1.00	2.50	O'Brien et al. 2020

27.3 - 26.3 Ma

Site	Latitude	Longitude	Event	Average Age (Ma)	Proxy	Number of Data points	Paleolatitude	Lowest Latitude	Highest Latitude	Min Latitudinal error	Max Latitudinal error	Average SST (°C)	Standard deviation (°C)	Analytical error (°C)	Calibration error (°C)	References
336	63.35	-7.79	MOGI	26.8	UK37	1	57.4	54.81	60.01	2.5	2.7	14.77	0.00	0.30	1.50	Liu et al. 2009
511	-51.00	-46.97	MOGI	26.8	TEX86	1	-57.0	-59.67	-54.47	2.7	2.5	17.54	0.00	1.00	2.50	Liu et al. 2009, Houben et al. 2019
516	-30.28	-35.29	MOGI	26.8	TEX86	6	-35.8	-38.51	-33.31	2.7	2.5	27.87	0.41	1.00	2.50	O'Brien et al. 2020
274	-69.00	173.43	MOGI	26.8	TEX86	6	-64.9	-67.57	-62.37	2.6	2.6	12.31	0.33	1.00	2.50	Hoem et al. 2021
1356	-63.31	136.00	MOGI	26.8	TEX86	5	-58.5	-61.14	-55.94	2.6	2.6	19.68	1.89	1.00	2.50	Hartman et al. 2018
1168	-42.61	144.41	MOGI	26.8	UK37	9	-52.6	-55.23	-50.03	2.7	2.5	23.69	1.44	0.30	1.50	Guitian & Stoll 2021, Hoem et al. 2022
1404	40.01	-51.81	MOGI	26.8	UK37	8	33.7	31.15	36.36	2.5	2.7	24.95	0.48	0.30	1.50	Liu et al. 2018
925	4.20	-43.49	MOGI	26.8	TEX86	1	-1.7	-4.36	0.85	2.6	2.6	25.64	0.00	1.00	2.50	Liu et al. 2009, Zhang et al. 2013, Inglis et al. 2015, Cramwinckel et al. 2018
1406	40.35	-51.65	MOGI	26.8	UK37, TEX86	4	34.0	31.48	36.68	2.5	2.7	25.86	1.15	1.00	2.50	Guitian et al. 2019
929	5.98	-43.74	MOGI	26.8	TEX86	17	0.0	-2.59	2.62	2.6	2.6	28.72	1.08	1.00	2.50	O'Brien et al. 2020, Liu et al. 2009
608	42.84	-23.09	MOGI	26.8	TEX86	2	36.5	33.97	39.18	2.5	2.7	30.57	1.52	1.00	2.50	Super et al. 2018
690	-65.16	1.20	MOGI	26.8	d18O	4	-68.4	-71.06	-65.86	2.6	2.6	5.03	0.77	1.00	2.50	Ehrmann & Mackensen 1992, Gaskell et al. 2022

33.7 - 33.2 Ma

Site	Latitude	Longitude	Event	Average Age (Ma)	Proxy	Number of Data points	Paleolatitude	Lowest Latitude	Highest Latitude	Min Latitudinal error	Max Latitudinal error	Average SST (°C)	Standard deviation (°C)	Analytical error (°C)	Calibration error (°C)	References
274	-69.00	173.43	EOGM	33.4	TEX86	1	-64.6	-67.31	-61.91	2.7	2.7	11.91	0.00	1.00	2.50	Hoem et al. 2021
511	-51.00	-46.97	EOGM	33.4	UK37, TEX86	13	-58.0	-60.77	-55.36	2.8	2.6	12.94	3.29	1.00	2.50	Liu et al. 2009, Plancq et al. 2014, Houben et al. 2019
913	75.49	6.95	EOGM	33.4	UK37	2	67.4	64.76	70.17	2.7	2.7	15.51	4.80	0.30	1.50	Liu et al. 2009
1356	-63.31	136.00	EOGM	33.4	TEX86	1	-58.0	-60.74	-55.34	2.8	2.6	19.87	0.00	1.00	2.50	Hartman et al. 2018
1168	-42.61	144.41	EOGM	33.4	TEX86	5	-55.3	-58.07	-52.67	2.8	2.6	24.92	0.83	1.00	2.50	Hoem et al. 2022
1404	40.01	-51.81	EOGM	33.4	UK37	13	32.5	29.90	35.31	2.6	2.8	26.30	0.78	0.30	1.50	Liu et al. 2018
1209	32.65	158.51	EOGM	33.4	TEX86	2	29.8	27.20	32.61	2.6	2.8	26.42	0.06	1.00	2.50	Kast et al. 2019
959	3.63	-2.74	EOGM	33.4	TEX86	6	-4.2	-6.95	-1.54	2.7	2.7	26.63	0.46	1.00	2.50	Cramwinckel et al. 2018
925	4.20	-43.49	EOGM	33.4	TEX86, d18O	4	-2.7	-5.45	-0.03	2.7	2.7	30.41	1.13	1.00	2.50	Liu et al. 2009, Zhang et al. 2013, Inglis et al. 2015, Cramwinckel et al. 2018, Tremblin et al. 2016
744	-61.58	80.60	EOGM	33.4	d18O	6	-58.3	-61.08	-55.67	2.8	2.6	6.70	1.41	1.00	2.50	Barron et al. 1991; Gaskell 2022

Table A3: Summary of all compiled sea surface temperatures (SSTs) for all Site locations including the analytical and calibration errors used for each proxy. Top: Available SST data for the Oligocene Miocene Transition (OMT), Middle: Available SST data for the Mid Oligocene Glacial Interval (MOGI), Bottom: Available SST data for the Eocene Oligocene Glacial Maximum (EOGM).

33.9-33 Ma													True value		True value + Error		
Locality/Sample ID	Age (Ma)	Paleolatitude (33Ma)	Paleolongitude (33Ma)	Proxy	Error (°C)	Mean (°C)	Median (°C)	Lower quartile (°C)	LQ + Error (°C)	Upper quartile (°C)	UQ + Error (°C)		Min value (°C)	Max value (°C)	Min value (°C)	Max value (°C)	Reference
Cervera	27.8-33.9	38.44	2.43	NLR	1.8	16.3	16.1	14.5	12.7	18.0	19.7		13.6	18.9	11.8	20.7	Tosal & Martín-Closas 2016
Daxing'anling	28.4- 33.9	43.73	120.42	NLR	2.3	10.3	10.3	8.7	6.3	13.2	15.5		8.0	13.6	5.7	15.9	Ma et al. 2012
IODP1168A	22.9-34.9	-62.90	149.63	TEX_{86}	0.9	25.4	25.6	25.0	24.1	26.0	26.9		23.7	26.4	22.8	27.3	Hoem et al. 2022
ODP 274	24.5-33.7	-70.24	177.16	TEX_{86}	0.7	12.4	12.4	12.1	11.4	12.6	13.3		11.9	12.8	11.3	13.5	Hoem et al. 2021
ODP744	24.1-34.9	-63.68	75.30	$\delta^{18}O$	1.9	7.9	8.2	6.6	4.7	8.7	10.6		4.6	11.1	2.7	13.0	Barrera & Huber 1991, Gaskell 2022
Paleogene basin	27-33.9	42.08	14.10	NLR	1.6	16.2	16.1	14.2	12.6	17.5	19.1		12.8	18.9	11.2	20.5	Erdei et al. 2012
Roudníky area	30-33.9	46.27	15.68	NLR	1.8	14.1	14.4	12.6	10.8	16.2	18.0		11.2	16.8	9.4	18.6	Kvaček & Walther 1995
Tard Clay	32-33.8	42.71	19.85	NLR	2.4	16.9	16.9	14.6	12.2	19.4	21.8		14.6	19.4	12.2	21.8	Kvaček et al. 2001
Upper Ruby Basin	32.2-33.6	51.56	-115.06	NLR	1.7	13.5	13.3	11.6	9.9	15.0	16.7		10.2	16.8	8.5	18.5	Becker 1966

33-26.5 Ma													True value		True value + Error		
Locality/Sample ID	Age (Ma)	Paleolatitude (30Ma)	Paleolongitude (30Ma)	Proxy	Error (°C)	Mean (°C)	Median (°C)	Lower quartile (°C)	LQ + Error (°C)	Upper quartile (°C)	UQ + Error (°C)		Min value (°C)	Max value (°C)	Min value (°C)	Max value (°C)	Reference
As Pontes basin	22.4-29.8	41.37	-6.13	NLR	3.3	14.8	14.8	11.2	7.9	17.7	21.0		11.2	17.7	7.9	21.0	Cabrera et al. 1994
Belen Fruit & Seed assemblage	30-28.5	0.05	-84.71	NLR	1.1	25.2	25.2	23.7	22.6	25.9	27.0		23.7	25.9	22.6	27.0	Manchester et al. 2012
Calau Beds	28-31	47.80	15.65	NLR	1.8	15.4	15.6	13.3	11.5	16.8	18.6		11.3	19.2	9.5	21.0	Ferguson et al. 2010
Cervera	27.8-33.9	41.65	1.33	NLR	1.8	16.3	16.1	14.5	12.7	18.0	19.7		13.6	18.9	11.8	20.7	Tosal & Martín-Closas 2016
Daxing'anling	28.4- 33.9	44.03	121.21	NLR	2.3	10.3	10.3	8.7	6.3	13.2	15.5		8.0	13.6	5.7	15.9	Ma et al. 2012
Guang River	27.23	7.31	34.03	NLR	1.4	24.3	24.3	22.8	21.4	25.5	26.9		22.8	25.5	21.4	26.9	Pan 2007
Haselbach Horizon	29-30.5	47.48	14.95	NLR	1.5	15.9	15.6	14.1	12.6	17.1	18.7		12.8	18.8	11.3	20.3	Kunzmann & Walther 2012
Haynes Creek Flora	30	50.89	-116.83	NLR	1.9	11.5	11.4	9.6	7.7	13.3	15.2		8.0	13.9	6.1	15.8	Axelrod 1998
Hrazený hill	28-31	46.94	16.09	NLR	1.9	12.9	13.2	11.7	9.8	15.3	17.2		9.1	16.2	7.2	18.1	Kvaček et al. 2015
IODP1168A	22.9-34.9	-60.95	148.67	TEX_{86}	1.4	25.3	25.4	24.6	23.3	26.4	27.7		21.9	27.9	20.5	29.3	Hoem et al. 2022
IODP1168A	22.9-29.2	-60.95	148.67	U^{K}_{37}	1.5	21.3	21.1	20.4	18.9	22.1	23.6		19.2	23.4	17.7	24.9	Guitian & Stoll, 2021
Kraskino Flora	30	40.09	122.70	NLR	1.6	18.5	18.8	16.9	15.3	20.2	21.9		14.5	22.2	12.9	23.8	Pavlyutkin 2011
Lea River	30-32	-59.66	149.94	NLR	2.2	10.2	10.2	8.2	6.0	12.6	14.8		8.2	12.6	6.0	14.8	Paull & Hill 2010
Makum Coal Field	23-29.4	24.42	92.74	NLR	1.2	24.3	23.9	23.5	22.3	25.8	27.0		23.1	26.4	21.9	27.6	Awasthi & Mehrotra 1995
ODP 274	24.5-33.7	-70.03	176.95	TEX_{86}	1.2	13.5	13.3	12.5	11.3	14.6	15.8		11.4	15.7	10.2	17.0	Hoem et al. 2021
ODP690	24.2-30.1	-64.25	-5.70	$\delta^{18}O$	1.2	4.6	4.5	3.7	2.6	5.6	6.7		3.1	6.2	2.0	7.4	Mackensen & Ehrmann 1992, Gaskell 2022
ODP744	24.1-34.9	-63.58	75.92	$\delta^{18}O$	1.2	7.0	6.9	6.0	4.8	7.8	8.9		5.3	9.6	4.1	10.8	Barrera & Huber 1991, Gaskell 2022
Paleogene basin	27-33.9	42.44	14.05	NLR	1.6	16.2	16.1	14.2	12.6	17.5	19.1		12.8	18.9	11.2	20.5	Erdei et al. 2012
Pitch-Pinnacle flora	29-32.9	44.93	-108.88	NLR	1.7	12.4	12.4	10.6	8.9	13.9	15.6		10.6	13.9	8.9	15.6	Gregory & McIntosh 1996
Rauenberg	27-32	45.68	10.51	NLR	1.8	15.3	15.1	13.6	11.8	17.2	19.0		12.3	18.7	10.5	20.5	Mai 1998
Roudníky area	30-33.9	46.65	15.57	NLR	1.8	14.1	14.4	12.6	10.8	16.2	18.0		11.2	16.8	9.4	18.6	Kvaček & Walther 1995
Suletice-Berand	26-29	46.59	15.82	NLR	1.8	14.5	14.5	12.6	10.8	16.1	17.9		12.6	16.1	10.8	17.9	Cabrera et al. 1994
Tard Clay	32-33.8	43.17	19.82	NLR	2.4	16.9	16.9	14.6	12.2	19.4	21.8		14.6	19.4	12.2	21.8	Kvaček et al. 2001
Upper Ruby Basin	32.2-33.6	50.98	-114.80	NLR	1.7	13.5	13.3	11.6	9.9	15.0	16.7		10.2	16.8	8.5	18.5	Becker 1966
Weisselster	29-30.5	47.48	14.95	NLR	1.7	13.9	13.5	12.4	10.7	15.6	17.3		10.0	18.9	8.3	20.6	Gastaldo et al. 1998

25-23 Ma													True value		True value + Error		
Locality/Sample ID	Age (Ma)	Paleolatitude (24Ma)	Paleolongitude (24Ma)	Proxy	Error (°C)	Mean (°C)	Median (°C)	Lower quartile (°C)	LQ + Error (°C)	Upper quartile (°C)	UQ + Error (°C)		Min value (°C)	Max value (°C)	Min value (°C)	Max value (°C)	Reference
As Pontes basin	22.4-29.8	41.80	-6.44	NLR	3.3	14.8	14.8	11.2	7.9	17.7	21.0		11.2	17.7	7.9	21.0	Cabrera et al. 1994
Berwick Quarry	25	-52.34	147.39	NLR	1.2	15.9	15.6	14.5	13.3	16.7	17.9		13.0	18.8	11.8	20.0	Gastaldo et al. 1998
Cosy Dell	24.4-25.4	-44.80	170.69	NLR	1.3	15.8	15.7	14.3	13.0	16.8	18.1		12.6	17.8	11.3	19.1	Conran et al. 2014
IODP1168A	22.9-34.9	-57.00	147.14	TEX_{86}	2.3	24.6	25.2	23.0	20.7	26.4	28.7		18.5	27.9	16.2	30.3	Hoem et al. 2022
IODP1168A	22.9-29.2	-57.00	147.14	U^{K}_{37}	1.7	25.3	25.7	24.2	22.5	26.3	28.0		22.6	28.1	20.9	29.8	Guitian & Stoll, 2021
Maikop Group	25Ma	35.96	47.13	NLR	1.7	12.8	12.8	10.9	9.2	14.2	15.9		10.1	15.6	8.4	17.3	Popov et al. 2008
Makum Coal Field	23-29.4	25.46	93.70	NLR	1.2	24.3	23.9	23.5	22.3	25.8	27.0		23.1	26.4	21.9	27.6	Awasthi & Mehrotra 1995
Monpeelyata deposit	22.4-24.2	-55.94	149.71	NLR	1.9	13.3	13.3	11.1	9.1	14.9	16.8		10.5	15.9	8.6	17.8	Macphail et al. 1991
Newvale Mine	23-25.2	-51.28	-174.24	NLR	1.3	15.7	15.9	14.4	13.1	17.0	18.4		11.8	19.1	10.5	20.4	Conran et al. 2014
ODP 274	24.5-33.7	-69.65	176.37	TEX_{86}	0.8	12.7	12.8	12.2	11.4	13.2	14.1		11.6	13.3	10.8	14.2	Hoem et al. 2021
ODP744	24.1-34.9	-63.36	77.13	$\delta^{18}O$	3.3	7.9	6.3	6.1	2.8	8.1	11.4		6.1	12.8	2.8	16.0	Barrera & Huber 1991, Gaskell 2022
San Julian Fm	24	-45.93	-74.05	NLR	1.7	16.4	16.4	14.7	13.0	18.0	19.7		14.7	18.0	13.0	19.7	Palazzesi & Barreda 2007

Table A4: All sea surface temperature (SST) data per Site location that was added to the O'Brien et al. 2020 Data-Model comparison. Including standard deviations and lower quartile (LQ) and upper quartile (UQ) errors. Top: All available SST data between 33.9 - 33 Ma; Middle: All available SST data between 22 – 26.5 Ma, Bottom: All available SST data between 25 – 23 Ma.

33.9-33 Ma												True value		True value + Error		
Locality/Sample ID	Age (Ma)	Paleolatitude (33Ma)	Paleolongitude (33Ma)	Proxy	Error (mm/yr)	Mean (mm/yr)	Median (mm/yr)	Lower quartile (mm/yr)	LQ + Error (mm/yr)	Upper quartile (mm/yr)	UQ + Error (mm/yr)	Min value (mm/yr)	Max value (mm/yr)	Min value (mm/yr)	Max value (mm/yr)	Reference
Cervera	27.8-33.9	38.44	2.43	NLR	196.6	955	933	759	562.0	1148	1344.7	660.7	1318.3	464.1	1514.8	Tosal & Martín-Closas 2016
Daxing'anling	28.4- 33.9	43.73	120.42	NLR	174.6	843	832	714	539.9	1057	1231.4	691.8	1096.5	517.2	1271.1	Ma et al. 2012
Paleogene basin	27-33.9	42.08	14.10	NLR	212.7	1107	1096	920	707.7	1343	1555.5	871.0	1380.4	658.3	1593.1	Erdei et al. 2012
Roudníky area	30-33.9	46.27	15.68	NLR	200.7	1102	1072	912	711.3	1306	1506.9	831.8	1380.4	631.0	1581.1	Kvaček & Walther 1995
Tard Clay	32-33.8	42.71	19.85	NLR	348.4	1000	1000	759	410.1	1445	1793.9	758.6	1445.4	410.1	1793.9	Kvaček et al. 2001
Upper Ruby Basin	32.2-33.6	51.56	-115.06	NLR	169.0	1028	1023	879	710.0	1213	1382.4	794.3	1318.3	625.3	1487.3	Becker 1966
33-26.5 Ma												**True value**		**True value + Error**		
Locality/Sample ID	**Age (Ma)**	**Paleolatitude (30Ma)**	**Paleolongitude (30Ma)**	**Proxy**	**Error (mm/yr)**	**Mean (mm/yr)**	**Median (mm/yr)**	**Lower quartile (mm/yr)**	**LQ + Error (mm/yr)**	**Upper quartile (mm/yr)**	**UQ + Error (mm/yr)**	**Min value (mm/yr)**	**Max value (mm/yr)**	**Min value (mm/yr)**	**Max value (mm/yr)**	**Reference**
As Pontes basin	22.4-29.8	41.37	-6.13	NLR	281	1000	1000	759	478	1318	1599	759	1318	477.9	1599.0	Cabrera et al. 1994
Belen Fruit & Seed assemblage	30-28.5	0.05	-84.71	NLR	322.4	1738	1738	1445	1123	2089	2411.7	1445.4	2089.3	1123.1	2411.7	Manchester et al. 2012
Calau Beds	28-31	47.80	15.65	NLR	195.4	1143	1122	973	777	1355	1550.6	912.0	1513.6	716.6	1708.9	Ferguson et al. 2010
Cervera	27.8-33.9	41.65	1.33	NLR	196.6	955	933	759	562	1148	1344.7	660.7	1318.3	464.1	1514.8	Tosal & Martín-Closas 2016
Daxing'anling	28.4- 33.9	44.03	121.21	NLR	174.6	843	832	714	540	1057	1231.4	691.8	1096.5	517.2	1271.1	Ma et al. 2012
Guang River	27.23	7.31	34.03	NLR	268.1	1445	1445	1202	934	1738	2005.9	1202.3	1737.8	934.1	2005.9	Pan 2007
Haselbach Horizon	29-30.5	47.48	14.95	NLR	209.9	1143	1175	973	763	1387	1596.6	871.0	1584.9	661.1	1794.8	Kunzmann & Walther 2012
Haynes Creek Flora	30	50.89	-116.83	NLR	170.6	891	912	755	584	1091	1262.1	691.8	1148.2	521.2	1318.8	Axelrod 1998
Hrazený hill	28-31	46.94	16.09	NLR	185.4	1038	1000	875	690	1242	1427.1	831.8	1380.4	646.4	1565.8	Kvaček et al. 2015
Kraskino Flora	30	40.09	122.70	NLR	214.0	1361	1380	1159	945	1585	1798.9	1096.5	1737.8	882.5	1951.8	Pavlyutkin 2011
Lea River	30-32	-59.66	149.94	NLR	369.0	1380	1380	1000	631	1738	2106.8	1000.0	1737.8	631.0	2106.8	Paull & Hill 2010
Makum Coal Field	23-29.4	24.42	92.74	NLR	331	1667	1660	1406	1075	2061	2391.8	1318.3	2290.9	987.1	2622.1	Awasthi & Mehrotra 1995
Paleogene basin	27-33.9	42.44	14.05	NLR	212.7	1107	1096	920	708	1343	1555.5	871.0	1380.4	658.3	1593.1	Erdei et al. 2012
Pitch-Pinnacle flora	29-32.9	44.93	-108.88	NLR	161.6	1047	1047	832	670	1148	1309.8	831.8	1148.2	670.2	1309.8	Gregory & McIntosh 1996
Rauenberg	27-32	45.68	10.51	NLR	222.9	1091	1072	871	648	1300	1523.0	794.3	1445.4	571.5	1668.3	Mai 1998
Roudníky area	30-33.9	46.65	15.57	NLR	200.7	1102	1072	912	711	1306	1506.9	831.8	1380.4	631.0	1581.1	Kvaček & Walther 1995
Suletice-Berand	26-29	46.59	15.82	NLR	255.3	1096	1096	871	616	1380	1635.7	871.0	1380.4	615.7	1635.7	Cabrera et al. 1994
Tard Clay	32-33.8	43.17	19.82	NLR	348.4	1000	1000	759	410	1445	1793.9	758.6	1445.4	410.1	1793.9	Kvaček et al. 2001
Upper Ruby Basin	32.2-33.6	50.98	-114.8	NLR	169.0	1028	1023	879	710	1213	1382.4	794.3	1318.3	625.3	1487.3	Becker 1966
Weisselster	29-30.5	47.48	14.95	NLR	181.3	1138	1096	955	774	1312	1493.5	871.0	1584.9	689.7	1766.2	Gastaldo et al. 1998
25-23 Ma												**True value**		**True value + Error**		
Locality/Sample ID	**Age (Ma)**	**Paleolatitude (24Ma)**	**Paleolongitude (24Ma)**	**Proxy**	**Error (mm/yr)**	**Mean (mm/yr)**	**Median (mm/yr)**	**Lower quartile (mm/yr)**	**LQ + Error (mm/yr)**	**Upper quartile (mm/yr)**	**UQ + Error (mm/yr)**	**Min value (mm/yr)**	**Max value (mm/yr)**	**Min value (mm/yr)**	**Max value (mm/yr)**	**Reference**
As Pontes basin	22.4-29.8	41.80	-6.44	NLR	281	1000	1000	759	478	1318	1599.0	758.6	1318.3	477.9	1599.0	Cabrera et al. 1994
Berwick Quarry	25	-52.34	147.39	NLR	310	1754	1820	1387	1077	1995	2305.2	1096.5	2187.8	786.5	2497.7	Gastaldo et al. 1998
Cosy Dell	24.4-25.4	-44.80	170.69	NLR	255	1556	1549	1288	1034	1786	2041.0	1202.3	1905.5	947.7	2160.0	Conran et al. 2014
Maikop Group	25Ma	35.96	47.13	NLR	173	1005	1000	843	670	1186	1358.7	758.6	1202.3	585.6	1375.2	Popov et al. 2008
Makum Coal Field	23-29.4	25.46	93.70	NLR	331	1667	1660	1406	1075	2061	2391.8	1318.3	2290.9	987.1	2622.1	Awasthi & Mehrotra 1995
Monpeelyata deposit	22.4-24.2	-55.94	149.71	NLR	274	1294	1349	1038	763	1585	1859.1	794.3	1819.7	520.1	2093.9	Macphail et al. 1991
Newvale Mine	23-25.2	-51.28	-174.24	NLR	258	1556	1585	1324	1066	1837	2094.4	1096.5	2187.8	838.6	2445.6	Conran et al. 2014
San Julian Fm	24	-45.93	-74.05	NLR	301	1202	1202	912	611	1514	1814.4	912.0	1513.6	611.2	1814.4	Palazzesi & Barreda 2007

Table A5: All precipitation (MAP) data per Site location that was used in the Data-Model comparison. Including standard deviations and lower quartile (LQ) and upper quartile (UQ) errors. Top: All available MAP data between 33.9 -33 Ma; Middle: All available MAP data between 22 – 26.5 Ma, Bottom: All available MAP data between 25 – 23 Ma.

8. Code Availability

All scripts and programs can be accessed via DOI: 10.5281/zenodo.10144091

9. Data Availability

All supplementary data is available via DOI: 10.5281/zenodo.10143889

10. Author Contribution

D.K.L.L.J. made the data compilation with C.L.O. The scripts and programs for the precipitation model were written by X.L., the scripts and programs for the sea surface temperature data were written by M.H.. T.R.. ran the nearest living analysis on compiled fossil plant remains. D.K.L.L.J. wrote the manuscript with P.K.B. and A.S. with contributions from all authors.

11. Competing Interests

Some authors are members of the editorial board of Climate of the Past.

12. Acknowledgements

We would like to thank both the editor and reviewers for their constructive feedback on our paper. This work was carried out under the program of the Netherlands Earth System Science Centre (NESSC), financially supported by the Ministry of Education, Culture and Science (OCW) through Gravitation Grant 024.002.001 and received funding from the European Union's Horizon 2020 research and innovation program under the Marie Skłodowska-Curie, grant agreement No. 847504.

13. References

Askin, R. A. and Raine, J. I.: Oligocene and Early Miocene Terrestrial Palynology of the Cape Roberts Drillhole CRP-2/2A, Victoria Land Basin, Antarctica, Terra Antartica, 7, 493–501, 2000.

Awasthi, N. and Mehrotra, R.: Oligocene flora from Makum Coalfield, Assam, India | Journal of Palaeosciences, Palaeobotanist, 44, 157–188, 1995.

Axelrod, D. I.: The Oligocene Haynes Creek Flora of Eastern Idaho, University of California Press, 164 pp., 1998.

Baatsen, M., van Hinsbergen, D. J. J., von der Heydt, A. S., Dijkstra, H. A., Sluijs, A., Abels, H. A., and Bijl, P. K.: Reconstructing geographical boundary conditions for palaeoclimate modelling during the Cenozoic, Climate of the Past, 12, 1635–1644, https://doi.org/10.5194/cp-12-1635-2016, 2016.

Baatsen, M., von der Heydt, A. S., Huber, M., Kliphuis, M. A., Bijl, P. K., Sluijs, A., and Dijkstra, H. A.: The middle-to-late Eocene greenhouse climate, modelled using the CESM 1.0.5, Climate of the Past, 16, 2573–2597, https://doi.org/10.5194/cp-2020-29, 2020.

Baatsen, M., Bijl, P., von der Heydt, A., Sluijs, A., and Dijkstra, H.: Resilient Antarctic monsoonal climate prevented ice growth during the Eocene, Climate of the Past, 20, 77–90, https://doi.org/10.5194/cp-20-77-2024, 2024.

Barker, P. F. and Burrell, J.: The opening of Drake Passage, Marine Geology, 25, 15–34, https://doi.org/10.1016/0025-3227(77)90045-7, 1977.

Barron, J. A., Baldauf, J. G., Barrera, E., Caulet, J. P., Huber, B. T., Keating, B. T., Lazarus, D., Sakai, H., Thierstein, H. R., and Wei, W.: Biochronologic and magnetochronologic synthesis of Leg 119 sediments from the Kerguelen Plateau and Prydz Bay, Antarctica, in: Barron, J., Larsen, B., et al., Proc. ODP, Sci. Results (Vol. 119, pp. 813-847), 813–847, 1991.

Becker, H. F.: Additions to and Revision of the Oligocene Ruby Paper Shale Flora of Southwestern Montana, Contributions from the Museum of Paleontology, 20, 89–119, 1966.

Beddow, H. M., Liebrand, D., Wilson, D. S., Hilgen, F. J., Sluijs, A., Wade, B. S., and Lourens, L. J.: Astronomical tunings of the Oligocene-Miocene transition from Pacific Ocean Site U1334 and implications for the carbon cycle, Clim. Past, 14, 255–270, https://doi.org/10.5194/cp-14-255-2018, 2018.

Bijl, P. K., Bendle, J. A. P., Bohaty, S. M., Pross, J., Schouten, S., Tauxe, L., Stickley, C. E., McKay, R. M., Roȟl, U., Olney, M., Sluijs, A., Escutia, C., and Brinkhuis, H.: Eocene cooling linked to early flow across the Tasmanian Gateway, Proc. Natl. Acad. Sci. U.S.A., 110, 9645–9650, https://doi.org/10.1073/pnas.1220872110, 2013.

Bijl, P. K., Frieling, J., Cramwinckel, M. J., Boschman, C., Sluijs, A., and Peterse, F.: Maastrichtian–Rupelian paleoclimates in the southwest Pacific – a critical re-evaluation of biomarker paleothermometry and dinoflagellate cyst paleoecology at Ocean Drilling Program Site 1172, Clim. Past, 17, 2393–2425, https://doi.org/10.5194/cp-17-2393-2021, 2021.

Billups, K., Channell, J. E. T., and Zachos, J.: Late Oligocene to early Miocene geochronology and paleoceanography from the subantarctic South Atlantic, Paleoceanography, 17, 4-1-4–11, https://doi.org/10.1029/2000PA000568, 2002.

Briard, J., Pucéat, E., Vennin, E., Daëron, M., Chavagnac, V., Jaillet, R., Merle, D., and de Rafélis, M.: Seawater paleotemperature and paleosalinity evolution in neritic environments of the Mediterranean margin: Insights from isotope analysis of bivalve shells, Palaeogeography, Palaeoclimatology, Palaeoecology, 543, 109582, https://doi.org/10.1016/j.palaeo.2019.109582, 2020.

Burke, K. D., Williams, J. W., Chandler, M. A., Haywood, A. M., Lunt, D. J., and Otto-Bliesner, B. L.: Pliocene and Eocene provide best analogs for near-future climates, Proc. Natl. Acad. Sci. U.S.A., 115, 13288–13293, https://doi.org/10.1073/pnas.1809600115, 2018.

Burls, N. J., Bradshaw, C. D., De Boer, A. M., Herold, N., Huber, M., Pound, M. J., Donnadieu, Y., Farnsworth, A., Frigola, A., Gasson, E., Von Der Heydt, A. S., Hutchinson, D. K., Knorr, G., Lawrence, K. T., Lear, C. H., Li, X., Lohmann, G., Lunt, D. J., Marzocchi, A., Prange, M., Riihimaki, C. A., Sarr, A. C., Siler, N., and Zhang, Z.: Simulating Miocene Warmth: Insights From an Opportunistic Multi-Model Ensemble (MioMIP1), Paleoceanography and Paleoclimatology, 36, 40, https://doi.org/10.1029/2020PA004054, 2021.

Cabrera, L., Hagemann, H. W., Pickel, W., and Sáez, A.: The coal-bearing, Cenozoic As Pontes basin (northwestern Spain) : geological influence on coal characteristics, International Journal of Coal Geology, 27, 201–226, https://doi.org/10.1016/0166-5162(94)00021-Q, 1995.

Clark, P. U., Shakun, J. D., Marcott, S. A., Mix, A. C., Eby, M., Kulp, S., Levermann, A., Milne, G. A., Pfister, P. L., Santer, B. D., Schrag, D. P., Solomon, S., Stocker, T. F., Strauss, B. H., Weaver, A. J., Winkelmann, R., Archer, D., Bard, E., Goldner, A., Lambeck, K., Pierrehumbert, R. T., and Plattner, G.-K.: Consequences of twenty-first-century policy for multi-millennial climate and sea-level change, Nature Clim Change, 6, 360–369, https://doi.org/10.1038/nclimate2923, 2016.

Coccioni, R., Montanari, A., Bice, D., Brinkhuis, H., Deino, A., Frontalini, F., Lirer, F., Maiorano, P., Monechi, S., Pross, J., Rochette, P., Sagnotti, L., Sideri, M., Sprovieri, M., Tateo, F., Touchard, Y., Simaeys, S. V., and Williams, G. L.: The Global Stratotype Section and Point (GSSP) for the base of the Chattian Stage (Paleogene System, Oligocene Series) at Monte Cagnero, Italy, Episodes, 41, 17–32, https://doi.org/10.18814/epiiugs/2018/v41i1/018003, 2018.

Conran, J. G., Mildenhall, D. C., Lee, D. E., Lindqvist, J. K., Shepherd, C., Beu, A. G., Bannister, J. M., and Stein, J. K.: Subtropical rainforest vegetation from Cosy Dell, Southland: Plant fossil evidence for Late Oligocene terrestrial ecosystems, New Zealand Journal of Geology and Geophysics, 57, 236–252, https://doi.org/10.1080/00288306.2014.888357, 2014.

Couvreur, T. L. P., Dauby, G., Blach-Overgaard, A., Deblauwe, V., Dessein, S., Droissart, V., Hardy, O. J., Harris, D. J., Janssens, S. B., Ley, A. C., Mackinder, B. A., Sonké, B., Sosef, M. S. M., Stévart, T., Svenning, J., Wieringa, J. J., Faye, A., Missoup, A. D., Tolley, K. A., Nicolas, V., Ntie, S., Fluteau, F., Robin, C., Guillocheau, F., Barboni, D., and Sepulchre, P.: Tectonics, climate and the diversification of the tropical African terrestrial flora and fauna, Biol Rev, 96, 16–51, https://doi.org/10.1111/brv.12644, 2021.

Cox, M. D.: An Idealized Model of the World Ocean. Part I: The Global-Scale Water Masses, Journal of Physical Oceanography, 19, 1730–1752, 1989.

Coxall, H. K. and Pearson, P. N.: The Eocene – Oligocene Transition, Geological Society London, Special Publications, 2, 351–387, 2007.

Coxall, H. K. and Wilson, P. A.: Early Oligocene glaciation and productivity in the eastern equatorial Pacific: Insights into global carbon cycling, Paleoceanography, 26, 1–18, https://doi.org/10.1029/2010PA002021, 2011.

Crameri, F., Magni, V., Domeier, M., Shephard, G. E., Chotalia, K., Cooper, G., Eakin, C. M., Grima, A. G., Gürer, D., Király, Á., Mulyukova, E., Peters, K., Robert, B., and Thielmann, M.: A transdisciplinary and community-driven database to unravel subduction zone initiation, Nat Commun, 11, 3750, https://doi.org/10.1038/s41467-020-17522-9, 2020.

Cramwinckel, M., Burls, N. J., Fahad, A. A., Knapp, S., West, C. K., Reichgelt, T., Greenwood, D. R., Chan, W.-L., Donnadieu, Y., Hutchinson, D., De Boer, A. M., Ladant, J.-B., Morozova, P., Niezgodzki, I., Knorr, G., Steinig, S., Zhang, Z., Zhu, J., Feng, R., Lunt, D. J., Abe-Ouchi, A., and Inglis, G. N.: Global- and regional-scale hydrological response to early Eocene warmth, , https://doi.org/10.1002/essoar.10512308.1, 2022.

Cramwinckel, M. J., Huber, M., Kocken, I. J., Agnini, C., Bijl, P. K., Bohaty, S. M., Frieling, J., Goldner, A., Hilgen, F. J., Kip, E. L., Peterse, F., van der Ploeg, R., Röhl, U., Schouten, S., and Sluijs, A.: Synchronous tropical and polar temperature evolution in the Eocene, Nature, 559, 382–386, https://doi.org/10.1038/s41586-018-0272-2, 2018.

Creech, J. B., Baker, J. A., Hollis, C. J., Morgans, H. E. G., and Smith, E. G. C.: Eocene sea temperatures for the mid-latitude southwest Pacific from Mg/Ca ratios in planktonic and benthic foraminifera, Earth and Planetary Science Letters, 299, 483–495, https://doi.org/10.1016/j.epsl.2010.09.039, 2010.

De Man, E. and Simaeys, S. V.: Late Oligocene Warming Event in the southern North Sea Basin: benthic foraminifera as paleotemperature proxies, Netherlands Journal of Geosciences, 83, 227–239, https://doi.org/10.1017/S0016774600020291, 2004.

De Man, E., Van Simaeys, S., Vandenberghe, N., Harris, W. B., and Wampler, J. M.: On the nature and chronostratigraphic position of the Rupelian and Chattian stratotypes in the southern North Sea basin, Episodes, 33, 3–14, https://doi.org/10.18814/epiiugs/2010/v33i1/002, 2010.

De Vleeschouwer, D., Vahlenkamp, M., Crucifix, M., and Pälike, H.: Alternating Southern and Northern Hemisphere climate response to astronomical forcing during the past 35 m.y., Geology, 45, 375–378, https://doi.org/10.1130/G38663.1, 2017.

DeConto, R. M. and Pollard, D.: Rapid Cenozoic glaciation of Antarctica induced by declining atmospheric CO2, Nature, 421, 245–249, https://doi.org/10.1038/nature01290., 2003.

DeConto, R. M., Pollard, D., Wilson, P. A., Pälike, H., Lear, C. H., and Pagani, M.: Thresholds for Cenozoic bipolar glaciation, Nature, 455, 652–656, https://doi.org/10.1038/nature07337, 2008.

Dielforder, A.: Constraining the strength of megathrusts from fault geometries and application to the Alpine collision zone, Earth and Planetary Science Letters, 474, 49–58, https://doi.org/10.1016/j.epsl.2017.06.021, 2017.

Diester-Haass, L. and Zahn, R.: Eocene-Oligocene transition in the Southern Ocean: History of water mass circulation and biological productivity, Geology, 24, 163–166, 1996.

Ding, L., Spicer, R. A., Yang, J., Xu, Q., Cai, F., Li, S., Lai, Q., Wang, H., Spicer, T. E. V., Yue, Y., Shukla, A., Srivastava, G., Khan, M. A., Bera, S., and Mehrotra, R.: Quantifying the rise of the Himalaya orogen and implications for the South Asian monsoon, Geology, 45, 215–218, https://doi.org/10.1130/G38583.1, 2017.

Douglas, P. M. J., Affek, H. P., Ivany, L. C., Houben, A. J. P., Sijp, W. P., Sluijs, A., Schouten, S., and Pagani, M.: Pronounced zonal heterogeneity in Eocene southern high-latitude sea surface temperatures, Proc. Natl. Acad. Sci. U.S.A., 111, 6582–6587, https://doi.org/10.1073/pnas.1321441111, 2014.

Dumont, M. A.: Rapport sur la carte géologique du Royaume, Belgiquede l'Acade´mie royales des Sciences et des Lettres de la Belgique, 16, 351–373, 1849.

Dupont-Nivet, G., Krijgsman, W., Langereis, C. G., Abels, H. A., Dai, S., and Fang, X.: Tibetan plateau aridification linked to global cooling at the Eocene–Oligocene transition, Nature, 445, 635–638, https://doi.org/10.1038/nature05516, 2007.

Eagles, G.: Tectonic Reconstructions of the Southernmost Andes and the Scotia Sea During the Opening of the Drake Passage, in: Geodynamic Evolution of the Southernmost Andes, edited by: C. Ghiglione, M., Springer International Publishing, Cham, 75–108, https://doi.org/10.1007/978-3-319-39727-6_4, 2016.

Eagles, G. and Jokat, W.: Tectonic reconstructions for paleobathymetry in Drake Passage, Tectonophysics, 611, 28–50, https://doi.org/10.1016/j.tecto.2013.11.021, 2014.

Eldrett, J. S., Harding, I. C., Wilson, P. A., Butler, E., and Roberts, A. P.: Continental ice in Greenland during the Eocene and Oligocene, Nature, 446, 176–179, https://doi.org/10.1038/nature05591, 2007.

Eldrett, J. S., Greenwood, D. R., Harding, I. C., and Huber, M.: Increased seasonality through the Eocene to Oligocene transition in northern high latitudes, Nature, 459, 969–973, https://doi.org/10.1038/nature08069, 2009.

Erdei, B., Utescher, T., Hably, L., Tamás, J., Roth-Nebelsick, A., and Grein, M.: Early Oligocene Continental Climate of the Palaeogene Basin (Hungary and Slovenia) and the Surrounding Area, Turkish Journal of Earth Sciences, 21, 153–186, https://doi.org/10.3906/yer-1005-29, 2012.

Evangelinos, D., Escutia, C., Etourneau, J., Hoem, F., Bijl, P., Boterblom, W., van de Flierdt, T., Valero, L., Flores, J.-A., Rodriguez-Tovar, F. J., Jimenez-Espejo, F. J., Salabarnada, A., and López-Quirós, A.: Late Oligocene-Miocene proto-Antarctic Circumpolar Current dynamics off the Wilkes Land margin, East Antarctica, Global and Planetary Change, 191, 103221, https://doi.org/10.1016/j.gloplacha.2020.103221, 2020.

Evangelinos, D., Escutia, C., van de Flierdt, T., Valero, L., Flores, J.-A., Harwood, D. M., Hoem, F. S., Bijl, P., Etourneau, J., Kreissig, K., Nilsson-Kerr, K., Holder, L., López-Quirós, A., and Salabarnada, A.: Absence of a strong, deep-reaching Antarctic Circumpolar Current zonal flow across the Tasmanian gateway during the Oligocene to early Miocene, Global and Planetary Change, 208, 103718, https://doi.org/10.1016/j.gloplacha.2021.103718, 2022.

Evans, D., Sagoo, N., Renema, W., Cotton, L. J., Müller, W., Todd, J. A., Saraswati, P. K., Stassen, P., Ziegler, M., Pearson, P. N., Valdes, P. J., and Affek, H. P.: Eocene greenhouse climate revealed by coupled clumped isotope-Mg/Ca thermometry, Proc. Natl. Acad. Sci. U.S.A., 115, 1174–1179, https://doi.org/10.1073/pnas.1714744115, 2018.

Farnsworth, A., Lunt, D. J., O'Brien, C. L., Foster, G. L., Inglis, G. N., Markwick, P., Pancost, R. D., and Robinson, S. A.: Climate Sensitivity on Geological Timescales Controlled by Nonlinear Feedbacks and Ocean Circulation, Geophys. Res. Lett., 46, 9880–9889, https://doi.org/10.1029/2019GL083574, 2019.

Fenero, R., Cotton, L., Molina, E., and Monechi, S.: Micropalaeontological evidence for the late Oligocene Oi-2b global glaciation event at the Zarabanda section, Spain, Palaeogeography, Palaeoclimatology, Palaeoecology, 369, 1–13, https://doi.org/10.1016/j.palaeo.2012.08.020, 2013.

Ferguson, D. K., Lee, D. E., Bannister, J. M., Zetter, R., Jordan, G. J., Vavra, N., and Mildenhall, D. C.: The taphonomy of a remarkable leaf bed assemblage from the Late Oligocene–Early Miocene Gore Lignite Measures, southern New Zealand, International Journal of Coal Geology, 83, 173–181, https://doi.org/10.1016/j.coal.2009.07.009, 2010.

Fischer, H., Meissner, K. J., Mix, A. C., Abram, N. J., Austermann, J., Brovkin, V., Capron, E., Colombaroli, D., Daniau, A. L., Dyez, K. A., Felis, T., Finkelstein, S. A., Jaccard, S. L., McClymont, E. L., Rovere, A., Sutter, J., Wolff, E. W., Affolter, S., Bakker, P., Ballesteros-Cánovas, J. A., Barbante, C., Caley, T., Carlson, A. E., Churakova, O., Cortese, G., Cumming, B. F., Davis, B. A. S., De Vernal, A., Emile-Geay, J., Fritz, S. C., Gierz, P., Gottschalk, J., Holloway, M. D., Joos, F., Kucera, M., Loutre, M. F., Lunt, D. J., Marcisz, K., Marlon, J. R., Martinez, P., Masson-Delmotte, V., Nehrbass-Ahles, C., Otto-Bliesner, B. L., Raible, C. C., Risebrobakken, B., Sánchez Goñi, M. F., Arrigo, J. S., Sarnthein, M., Sjolte, J., Stocker, T. F., Velasquez Alvárez, P. A., Tinner, W., Valdes, P. J., Vogel, H., Wanner, H., Yan, Q., Yu, Z., Ziegler, M., and Zhou, L.: Palaeoclimate constraints on the impact of 2°C anthropogenic warming and beyond, Nature Geoscience, 11, 474–485, https://doi.org/10.1038/s41561-018-0146-0, 2018.

Flower, B. P., Zachos, J. C. C., and Paul, H.: Milankovitch-scale climate variability recorded near the Oligocene/Miocene boundary, Proceedings of the Ocean Drilling Program, 154, 433–439, https://doi.org/10.2973/odp.proc.sr.154.141.1997, 1997.

Fordyce, R. E.: Whale evolution and Oligocene southern ocean environments, Palaeogeography, Palaeoclimatology, Palaeoecology, 31, 319–336, https://doi.org/10.1016/0031-0182(80)90024-3, 1980.

Foster, G. L., Royer, D. L., and Lunt, D. J.: Future climate forcing potentially without precedent in the last 420 million years, Nat Commun, 8, 1–8, https://doi.org/10.1038/ncomms14845, 2017.

Fuchs, T.: Tertiärfossilien aus den kohlenführenden Miocaenablagerungen der Umgebung von Krapina und Radoboj und über die Stellung der sogenannten "Aquitanische Stufe.," Mitteilungen aus dem Jahrbuche der Kgl. Ungarischen Geologischen Anstalt, 10, 161–175, 1894.

Galeotti, S., DeConto, R., Naish, T., Stocchi, P., Florindo, F., Pagani, M., Barrett, P., Bohaty, S. M., Lanci, L., Pollard, D., Sandroni, S., Talarico, F. M., and Zachos, J. C.: Antarctic Ice Sheet variability across the Eocene-Oligocene boundary climate transition, Science, 352, 76–80, https://doi.org/www.sciencemag.org/content/352/6281/76/suppl/DC1, 2016.

Gaskell, D. E., Huber, M., O'Brien, C. L., Inglis, G. N., Acosta, R. P., Poulsen, C. J., and Hull, P. M.: The latitudinal temperature gradient and its climate dependence as inferred from foraminiferal $\delta^{18}O$ over the past 95 million years, Proc. Natl. Acad. Sci. U.S.A., 119, e2111332119, https://doi.org/10.1073/pnas.2111332119, 2022.

Gastaldo, R. A., Riegel, W., Püttmann, W., Linnemann, U. G., and Zetter, R.: A multidisciplinary approach to reconstruct the Late Oligocene vegetation in central Europe, Review of Palaeobotany and Palynology, 101, 71–94, https://doi.org/10.1016/S0034-6667(97)00070-5, 1998.

Goldner, A., Herold, N., and Huber, M.: Antarctic glaciation caused ocean circulation changes at the Eocene-Oligocene transition, Nature, 511, 574–577, https://doi.org/10.1038/nature13597, 2014.

Gradstein, F. M.: Introduction, in: Geologic Time Scale 2020, Elsevier, 3–20, https://doi.org/10.1016/B978-0-12-824360-2.00001-2, 2020.

Greenop, R., Sosdian, S. M., Henehan, M. J., Wilson, P. A., Lear, C. H., and Foster, G. L.: Orbital Forcing, Ice Volume, and CO_2 Across the Oligocene-Miocene Transition, Paleoceanography and Paleoclimatology, 34, 316–328, https://doi.org/10.1029/2018PA003420, 2019.

Gregory, K. M. and McIntosh, W. C.: Paleoclimate and paleoelevation of the Oligocene Pitch-Pinnacle flora, Sawatch Range, Colorado, Geol Soc America Bull, 108, 545–561, https://doi.org/10.1130/0016-7606(1996)108<0545:PAPOTO>2.3.CO;2, 1996.

Guitián, J. and Stoll, H. M.: Evolution of Sea Surface Temperature in the Southern Mid-latitudes From Late Oligocene Through Early Miocene, Paleoceanog and Paleoclimatol, 36, https://doi.org/10.1029/2020PA004199, 2021.

Guitián, J., Phelps, S., Polissar, P. J., Ausín, B., Eglinton, T. I., and Stoll, H. M.: Midlatitude Temperature Variations in the Oligocene to Early Miocene, Paleoceanography and Paleoclimatology, 34, 1328–1343, https://doi.org/10.1029/2019PA003638, 2019.

Hardenbol, J. and Berggren, W. A.: A New Paleogene Numerical Time Scale, American Association of Petroleum Geologists Studies in Geology, 6, 213–234, 1978.

Hartman, J. D., Sangiorgi, F., Salabarnada, A., Peterse, F., Houben, A. J. P., Schouten, S., Brinkhuis, H., Escutia, C., and Bijl, P. K.: Paleoceanography and ice sheet variability offshore Wilkes Land, Antarctica-Part 3: Insights from Oligocene-Miocene TEX86-based sea surface temperature reconstructions, Climate of the Past, 14, 1275–1297, https://doi.org/10.5194/cp-14-1275-2018, 2018.

Heureux, A. M. C. and Rickaby, R. E. M.: Refining our estimate of atmospheric CO 2 across the Eocene–Oligocene climatic transition, Earth and Planetary Science Letters, 409, 329–338, https://doi.org/10.1016/j.epsl.2014.10.036, 2015.

Hill, D. J., Haywood, A. M., Valdes, P. J., Francis, J. E., Lunt, D. J., Wade, B. S., and Bowman, V. C.: Paleogeographic controls on the onset of the Antarctic circumpolar current, Geophysical Research Letters, 40, 5199–5204, https://doi.org/10.1002/grl.50941, 2013.

van Hinsbergen, D. J. J.: Indian plate paleogeography, subduction and horizontal underthrusting below Tibet: paradoxes, controversies and opportunities, National Science Review, 9, nwac074, https://doi.org/10.1093/nsr/nwac074, 2022.

Ho, S. L. and Laepple, T.: Flat meridional temperature gradient in the early Eocene in the subsurface rather than surface ocean, Nature Geosci, 9, 606–610, https://doi.org/10.1038/ngeo2763, 2016.

Hoem, F. S., Valero, L., Evangelinos, D., Escutia, C., Duncan, B., McKay, R. M., Brinkhuis, H., Sangiorgi, F., and Bijl, P. K.: Temperate Oligocene surface ocean conditions offshore of Cape Adare, Ross Sea, Antarctica, Clim. Past, 17, 1423–1442, https://doi.org/10.5194/cp-17-1423-2021, 2021.

Hoem, F. S., Sauermilch, I., Aleksinski, A. K., Huber, M., Peterse, F., Sangiorgi, F., and Bijl, P. K.: Strength and variability of the Oligocene Southern Ocean surface temperature gradient, Commun Earth Environ, 3, 1–8, https://doi.org/10.1038/s43247-022-00666-5, 2022.

Holland, M. M. and Bitz, C. M.: Polar amplification of climate change in coupled models, Climate Dynamics, 21, 221–232, https://doi.org/10.1007/s00382-003-0332-6, 2003.

Hollis, C. J., Dunkley Jones, T., Anagnostou, E., Bijl, P. K., Cramwinckel, M. J., Cui, Y., Dickens, G. R., Edgar, K. M., Eley, Y., Evans, D., Foster, G. L., Frieling, J., Inglis, G. N., Kennedy, E. M., Kozdon, R., Lauretano, V., Lear, C. H., Littler, K., Lourens, L., Meckler, A. N., Naafs, B. D. A., Pälike, H., Pancost, R. D., Pearson, P. N., Röhl, U., Royer, D. L., Salzmann, U., Schubert, B. A., Seebeck, H., Sluijs, A., Speijer, R. P., Stassen, P., Tierney, J., Tripati, A., Wade, B., Westerhold, T., Witkowski, C., Zachos, J. C., Zhang, Y. G., Huber, M., and Lunt, D. J.: The DeepMIP contribution to PMIP4: methodologies for selection, compilation and analysis of latest Paleocene and early Eocene climate proxy data, incorporating version 0.1 of the DeepMIP database, Geosci. Model Dev., 12, 3149–3206, https://doi.org/10.5194/gmd-12-3149-2019, 2019.

Houben, A. J. P., van Mourik, C. A., Montanari, A., Coccioni, R., and Brinkhuis, H.: The Eocene-Oligocene transition: Changes in sea level, temperature or both?, Palaeogeography, Palaeoclimatology, Palaeoecology, 335–336, 75–83, https://doi.org/10.1016/j.palaeo.2011.04.008, 2012.

Houben, A. J. P., Bijl, P. K., Pross, J., Bohaty, S. M., Passchier, S., Stickley, C. E., Röhl, U., Sugisaki, S., Tauxe, L., van de Flierdt, T., Olney, M., Sangiorgi, F., Sluijs, A., Escutia, C., Brinkhuis, H., and and the Expedition 318 Scientists: Reorganization of Southern Ocean Plankton Ecosystem at the Onset of Antarctic Glaciation, Science, 340, 341–344, https://doi.org/10.1126/science.1223646, 2013.

Houben, A. J. P., Bijl, P. K., Sluijs, A., Schouten, S., and Brinkhuis, H.: Late Eocene Southern Ocean Cooling and Invigoration of Circulation Preconditioned Antarctica for Full-Scale Glaciation, Geochem. Geophys. Geosyst., 20, 2019GC008182, https://doi.org/10.1029/2019GC008182, 2019.

Huang, B., Banzon, V. F., Freeman, E., Lawrimore, J., Liu, W., Peterson, T. C., Smith, T. M., Thorne, P. W., Woodruff, S. D., and Zhang, H.-M.: Extended Reconstructed Sea Surface Temperature Version 4 (ERSST.v4). Part I: Upgrades and Intercomparisons, Journal of Climate, 28, 911–930, https://doi.org/10.1175/JCLI-D-14-00006.1, 2015.

Huber, M. and Caballero, R.: The early Eocene equable climate problem revisited, Clim. Past, 7, 603–633, https://doi.org/10.5194/cp-7-603-2011, 2011.

Huber, M., Brinkhuis, H., Stickley, C. E., Döös, K., Sluijs, A., Warnaar, J., Schellenberg, S. A., and Williams, G. L.: Eocene circulation of the Southern Ocean: Was Antarctica kept warm by subtropical waters?, Paleoceanography, 19, 1–12, https://doi.org/10.1029/2004PA001014, 2004.

Hurley, S. J., Lipp, J. S., Close, H. G., Hinrichs, K.-U., and Pearson, A.: Distribution and export of isoprenoid tetraether lipids in suspended particulate matter from the water column of the Western Atlantic Ocean, Organic Geochemistry, 116, 90–102, https://doi.org/10.1016/j.orggeochem.2017.11.010, 2018.

Hutchinson, D. K., de Boer, A. M., Coxall, H. K., Caballero, R., Nilsson, J., and Baatsen, M.: Climate sensitivity and meridional overturning circulation in the late Eocene using GFDL CM2.1, Clim. Past, 14, 789–810, https://doi.org/10.5194/cp-14-789-2018, 2018.

Hutchinson, D. K., Coxall, H. K., Lunt, D. J., Steinthorsdottir, M., de Boer, A. M., Baatsen, M., von der Heydt, A., Huber, M., Kennedy-Asser, A. T., Kunzmann, L., Ladant, J.-B., Lear, C. H., Moraweck, K., Pearson, P. N., Piga, E., Pound, M. J., Salzmann, U., Scher, H. D., Sijp, W. P., Śliwińska, K. K., Wilson, P. A., and Zhang, Z.: The Eocene–Oligocene transition: a review of marine and terrestrial proxy data, models and model–data comparisons, Clim. Past, 17, 269–315, https://doi.org/10.5194/cp-17-269-2021, 2021.

Inglis, G. N., Farnsworth, A., Lunt, D. J., Foster, G. L., Hollis, C. J., Pagani, M., Jardine, P. E., Pearson, P. N. P., Markwick, P., Galsworthy, A. M. J., Raynham, L., Taylor, K. W. R., and Pancost, R. D.: Descent toward the Icehouse: Eocene sea

surface cooling inferred from GDGT distributions, Paleoceanography, 30, 1000–1020, https://doi.org/10.1002/2014PA002723.Received, 2015.

IPCC: Climate Change 2022: Impacts, Adaptation and Vulnerability. Contribution of Working Group II to the Sixth Assessment Report of the Intergovernmental Panel on Climate Change [H.-O. Pörtner, D.C. Roberts, M. Tignor, E.S. Poloczanska, K. Mintenbeck, A. Alegría, M. Craig, S. Langsdorf, S. Löschke, V. Möller, A. Okem, B. Rama (eds.)]., 1st ed., Cambridge University Press, Cambridge, 3056 pp., https://doi.org/10.1017/9781009325844, 2022.

Jaramillo, C., Rueda, M. J., and Mora, G.: Cenozoic Plant Diversity in the Neotropics, Science, 311, 1893–1896, https://doi.org/10.1126/science.1121380, 2006.

Kast, E. R., Stolper, D. A., Auderset, A., Higgins, J. A., Ren, G. H., Wang, X., Martinez-Garcia, A., Haug, G. H., and Sigman, D. M.: Nitrogen isotope evidence for expanded ocean suboxia in the early Cenozoic, Paleoceanography, 364, 386–389, https://doi.org/10.1126/science.aau5784, 2019.

Kennedy, A. T., Farnsworth, A., Lunt, D. J., Lear, C. H., and Markwick, P. J.: Atmospheric and oceanic impacts of Antarctic glaciation across the Eocene–Oligocene transition, Phil. Trans. R. Soc. A., 373, 18, https://doi.org/10.1098/rsta.2014.0419, 2015.

Kennedy-Asser, A. T., Lunt, D. J., Farnsworth, A., and Valdes, P. J.: Assessing Mechanisms and Uncertainty in Modeled Climatic Change at the Eocene-Oligocene Transition, Paleoceanography and Paleoclimatology, 34, 16–34, https://doi.org/10.1029/2018PA003380, 2019.

Kennett, J. P.: Cenozoic evolution of Antarctic glaciation, the circum-Antarctic Ocean, and their impact on global paleoceanography, Journal of Geophysical Research, 82, 3843–3860, https://doi.org/10.1029/jc082i027p03843, 1977.

Kim, J.-H., van der Meer, J., Schouten, S., Helmke, P., Willmott, V., Sangiorgi, F., Koç, N., Hopmans, E. C., and Damsté, J. S. S.: New indices and calibrations derived from the distribution of crenarchaeal isoprenoid tetraether lipids: Implications for past sea surface temperature reconstructions, Geochimica et Cosmochimica Acta, 74, 4639–4654, https://doi.org/10.1016/j.gca.2010.05.027, 2010.

Kim, S.-T. and O'Neil, J. R.: Equilibrium and nonequilibrium oxygen isotope effects in synthetic carbonates, Geochimica et Cosmochimica Acta, 61, 3461–3475, https://doi.org/10.1016/S0016-7037(97)00169-5, 1997.

Köhler, P., De Boer, B., Von Der Heydt, A. S., Stap, L. B., and Van De Wal, R. S. W.: On the state dependency of the equilibrium climate sensitivity during the last 5 million years, Clim. Past, 11, 1801–1823, https://doi.org/10.5194/cp-11-1801-2015, 2015.

Kohn, M. J., Strömberg, C. A. E., Madden, R. H., Dunn, R. E., Evans, S., Palacios, A., and Carlini, A. A.: Quasi-static Eocene–Oligocene climate in Patagonia promotes slow faunal evolution and mid-Cenozoic global cooling, Palaeogeography, Palaeoclimatology, Palaeoecology, 435, 24–37, https://doi.org/10.1016/j.palaeo.2015.05.028, 2015.

Kotthoff, U., Greenwood, D. R., McCarthy, F. M. G., Müller-Navarra, K., Prader, S., and Hesselbo, S. P.: Late Eocene to middle Miocene (33 to 13 million years ago) vegetation and climate development on the North American Atlantic Coastal Plain (IODP Expedition 313, Site M0027), Clim. Past, 10, 1523–1539, https://doi.org/10.5194/cp-10-1523-2014, 2014.

Kováč, M.: The Central Paratethys palaeoceanography: a water circulation model based on microfossil proxies, climate, and changes of depositional environment, 41, 2017.

Kovar-Eder, J.: Early Oligocene plant diversity along the Upper Rhine Graben: The fossil flora of Rauenberg, Germany, Acta Palaeobotanica, 56, 329–440, https://doi.org/10.1515/acpa-2016-0011, 2016.

Kunzmann, L. and Walther, H.: Early Oligocene plant taphocoenoses of the Haselbach megafloral complex and the reconstruction of palaeovegetation, Palaeobio Palaeoenv, 92, 295–307, https://doi.org/10.1007/s12549-012-0078-4, 2012.

Kvacek, Z. and Walther, H.: The Oligocene Volcanic Flora of Suletice-Berand Near Ústí Nad Labem, North Bohemia - A review, Acta Musei Nationalis Pragae, 50, 25–54, 1995.

Kvaček, Z., Teodoridis, V., Mach, K., Přikryl, T., and Dvořák, Z.: Tracing the Eocene-Oligocene transition: A case study from North Bohemia, Bull. Geosci., 89, 1411, https://doi.org/10.3140/bull.geosci.1411, 2014.

Kvaček, Z., Teodoridis, V., and Zajícová, J.: Revision of the early Oligocene flora of Hrazený hill (formerly Pirskenberg) in Knížecí near Šluknov, North Bohemia, Acta Mus. Nat. Pragae ser.B, hist.nat., 71, 55–102, https://doi.org/10.14446/AMNP.2015.55, 2015.

Ladant, J.-B., Donnadieu, Y., Lefebvre, V., and Dumas, C.: The respective role of atmospheric carbon dioxide and orbital parameters on ice sheet evolution at the Eocene-Oligocene transition: Ice sheet evolution at the EOT, Paleoceanography, 29, 810–823, https://doi.org/10.1002/2013PA002593, 2014.

Laepple, T., Ziegler, E., Weitzel, N., Hébert, R., Ellerhoff, B., Schoch, P., Martrat, B., Bothe, O., Moreno-Chamarro, E., Chevalier, M., Herbert, A., and Rehfeld, K.: Regional but not global temperature variability underestimated by climate models at supradecadal timescales, Nat. Geosci., 16, 958–966, https://doi.org/10.1038/s41561-023-01299-9, 2023.

Lagabrielle, Y., Goddéris, Y., Donnadieu, Y., Malavieille, J., and Suarez, M.: The tectonic history of Drake Passage and its possible impacts on global climate, Earth and Planetary Science Letters, 279, 197–211, https://doi.org/10.1016/j.epsl.2008.12.037, 2009.

van de Lagemaat, S. H. A., Swart, M. L. A., Vaes, B., Kosters, M. E., Boschman, L. M., Burton-Johnson, A., Bijl, P. K., Spakman, W., and van Hinsbergen, D. J. J.: Subduction initiation in the Scotia Sea region and opening of the Drake Passage: When and why?, Earth-Science Reviews, 215, 103551, https://doi.org/10.1016/j.earscirev.2021.103551, 2021.

Laskarev, V.: Sur les équivalens du sarmatiien supérieur en Serbie, in: Receuil de traveaux offert à M. Jovan Cvijic par ses amis et collaborateurs, edited by: Vujević, P., Drzhavna Shtamparija, Belgrade, 73–85, 1924.

Levy, R. H., Meyers, S. R., Naish, T. R., Golledge, N. R., McKay, R. M., Crampton, J. S., DeConto, R. M., De Santis, L., Florindo, F., Gasson, E. G. W., Harwood, D. M., Luyendyk, B. P., Powell, R. D., Clowes, C., and Kulhanek, D. K.: Antarctic ice-sheet sensitivity to obliquity forcing enhanced through ocean connections, Nature Geosci, 12, 132–137, https://doi.org/10.1038/s41561-018-0284-4, 2019.

Liebrand, D., Beddow, H. M., Lourens, L. J., Pälike, H., Raffi, I., Bohaty, S. M., Hilgen, F. J., Saes, M. J. M., Wilson, P. A., van Dijk, A. E., Hodell, D. A., Kroon, D., Huck, C. E., and Batenburg, S. J.: Cyclostratigraphy and eccentricity tuning of the early Oligocene through early Miocene (30.1–17.1 Ma): Cibicides mundulus stable oxygen and carbon isotope records from Walvis Ridge Site 1264, Earth and Planetary Science Letters, 450, 392–405, https://doi.org/10.1016/j.epsl.2016.06.007, 2016.

Liebrand, D., De Bakker, A. T. M., Beddow, H. M., Wilson, P. A., Bohaty, S. M., Ruessink, G., Pälike, H., Batenburg, S. J., Hilgen, F. J., Hodell, D. A., Huck, C. E., Kroon, D., Raffi, I., Saes, M. J. M., Van Dijk, A. E., and Lourens, L. J.: Evolution of the early Antarctic ice ages, Proceedings of the National Academy of Sciences of the United States of America, 114, 3867–3872, https://doi.org/10.1073/pnas.1615440114, 2017.

Liu, Z., Tuo, S., Zhao, Q., Cheng, X., and Huang, W.: Deep-water Earliest Oligocene Glacial Maximum (EOGM) in South Atlantic, Chinese Sci Bull, 49, 2190–2197, https://doi.org/10.1360/04wd0228, 2004.

Liu, Z., Pagani, M., Zinniker, D., DeConto, R., Huber, M., Brinkhuis, H., Shah, S. R., Leckie, R. M., and Pearson, A.: Global Cooling During the Eocene-Oligocene Climate Transition, Science, 323, 1187–1190, https://doi.org/10.1126/science.1166368, 2009.

Liu, Z., He, Y., Jiang, Y., Wang, H., Liu, W., Bohaty, S. M., and Wilson, P. A.: Transient temperature asymmetry between hemispheres in the Palaeogene Atlantic Ocean, Nature Geosci, 11, 656–660, https://doi.org/10.1038/s41561-018-0182-9, 2018.

Lunt, D. J., Farnsworth, A., Loptson, C., Foster, G. L., Markwick, P., O'Brien, C. L., Pancost, R. D., Robinson, S. A., and Wrobel, N.: Palaeogeographic controls on climate and proxy interpretation, Clim. Past, 12, 1181–1198, https://doi.org/10.5194/cp-12-1181-2016, 2016.

Lunt, D. J., Bragg, F., Chan, W.-L., Hutchinson, D. K., Ladant, J.-B., Morozova, P., Niezgodzki, I., Steinig, S., Zhang, Z., Zhu, J., Abe-Ouchi, A., Anagnostou, E., de Boer, A. M., Coxall, H. K., Donnadieu, Y., Foster, G., Inglis, G. N., Knorr, G., Langebroek, P. M., Lear, C. H., Lohmann, G., Poulsen, C. J., Sepulchre, P., Tierney, J. E., Valdes, P. J., Volodin, E. M., Dunkley Jones, T., Hollis, C. J., Huber, M., and Otto-Bliesner, B. L.: DeepMIP: model intercomparison of early Eocene climatic optimum (EECO) large-scale climate features and comparison with proxy data, Climate of the Past, 17, 203–227, https://doi.org/10.5194/cp-17-203-2021, 2021.

Ma, X., Jiang, H., Cheng, J., and Xu, H.: Spatiotemporal evolution of Paleogene palynoflora in China and its implication for development of the extensional basins in East China, Review of Palaeobotany and Palynology, 184, 24–35, https://doi.org/10.1016/j.revpalbo.2012.07.013, 2012.

Macphail, M. K., Hill, R. S., Forsyth, S. M., and Wells, P. M.: A Late Oligocene-Early Miocene cool climate flora in Tasmania, Alcheringa: An Australasian Journal of Palaeontology, 15, 87–106, https://doi.org/10.1080/03115519108619011, 1991.

Mai, D. H.: Contribution to the flora of the middle Oligocene Calau Beds in Brandenburg, Germany, Review of Palaeobotany and Palynology, 101, 43–70, https://doi.org/10.1016/S0034-6667(97)00069-9, 1998.

Maldonado, A., Bohoyo, F., Galindo-Zaldívar, J., Hernández-Molina, F. J., Lobo, F. J., Lodolo, E., Martos, Y. M., Pérez, L. F., Schreider, A. A., and Somoza, L.: A model of oceanic development by ridge jumping: Opening of the Scotia Sea, Global and Planetary Change, 123, 152–173, https://doi.org/10.1016/j.gloplacha.2014.06.010, 2014.

Manchester, S. R., Herrera, F., Fourtanier, E., Barron, J., and Martinez, J.-N.: Oligocene Age of the Classic Belén Fruit and Seed Assemblage of North Coastal Peru based on Diatom Biostratigraphy, The Journal of Geology, 120, 467–476, https://doi.org/10.1086/665797, 2012.

Masson-Delmotte, V., Schulz, M., Abe-Ouchi, A., Beer, J., Ganopolski, A., Fidel, J., Rouco, G., Jansen, E., Lambeck, K., Luterbacher, J., Naish, T., Ramesh, R., Rojas, M., Shao, X., Anchukaitis, K., Arblaster, J., Bartlein, P. J., Benito, G., Clark, P., Comiso, J. C., Crowley, T., Deckker, P. D., de Vernal, A., Delmonte, B., DiNezio, P., Dowsett, H. J., Edwards, R. L., Fischer, H., Fleitmann, D., Foster, G., Fröhlich, C., Hall, A., Hargreaves, J., Haywood, A., Hollis, C., Krinner, G., Landais, A., Li, C., Lunt, D., Mahowald, N., McGregor, S., Meehl, G., Mitrovica, J. X., Moberg, A., Mudelsee, M., Muhs, D. R., Mulitza, S., Müller, S., Overland, J., Parrenin, F., Pearson, P., Robock, A., Rohling, E., Salzmann, U., Savarino, J., Sedláček, J., Shindell, D., Smerdon, J., Solomina, O., Tarasov, P., Vinther, B., Waelbroeck, C., Wolf, D., Yokoyama, Y., Yoshimori, M., Zachos, J., Zwartz, D., Gupta, A. K., Rahimzadeh, F., Raynaud, D., and Wanner, H.: Information from Paleoclimate

Archives, in: Climate Change 2013: The Physical Science Basis. Contribution of Working Group I to the Fifth Assessment Report of the Intergovernmental Panel on Climate Change, 2013.

Matsuura, K. and Willmott, C. J.: Terrestrial Air Temperature: 1900-2017 Gridded Monthly Time Series, 2018.

Meckler, A. N., Sexton, P. F., Piasecki, A. M., Leutert, T. J., Marquardt, J., Ziegler, M., Agterhuis, T., Lourens, L. J., Rae, J. W. B., Barnet, J., Tripati, A., and Bernasconi, S. M.: Cenozoic evolution of deep ocean temperature from clumped isotope thermometry, Science, 377, 86–90, https://doi.org/10.1126/science.abk0604, 2022.

Meschede, M. and Warr, L. N.: The Geology of Germany: A Process-Oriented Approach, Springer International Publishing, Cham, https://doi.org/10.1007/978-3-319-76102-2, 2019.

Miller, K. G., Feigenson, M. D., Kent, D. V., and Olsson, R. K.: Upper Eocene to Oligocene isotope (^{87}Sr/^{86}Sr, δ^{18}O, δ^{13}C) standard section, Deep Sea Drilling Project Site 522, Paleoceanography, 3, 223–233, https://doi.org/10.1029/PA003i002p00223, 1988.

Miller, K. G., Wright, J. D., and Fairbanks, R. G.: Unlocking the Ice House: Oligocene-Miocene oxygen isotopes, eustasy, and margin erosion, J. Geophys. Res., 96, 6829–6848, https://doi.org/10.1029/90JB02015, 1991.

Moraweck, K., Grein, M., Konrad, W., Kvaček, J., Kova-Eder, J., Neinhuis, C., Traiser, C., and Kunzmann, L.: Leaf traits of long-ranging Paleogene species and their relationship with depositional facies, climate and atmospheric CO2 level, palb, 298, 93–172, https://doi.org/10.1127/palb/2019/0062, 2019.

Müller, P. J., Kirst, G., Ruhland, G., von Storch, I., and Rosell-Melé, A.: Calibration of the alkenone paleotemperature index U37K′ based on core-tops from the eastern South Atlantic and the global ocean (60°N-60°S), Geochimica et Cosmochimica Acta, 62, 1757–1772, https://doi.org/10.1016/S0016-7037(98)00097-0, 1998.

Murphy, M. G. and Kennett, J. P.: Development of Latitudinal Thermal Gradients During the Oligocene: Oxygen Isotope Evidence from the Soutwest Pacific, Initial Reports of the DeepSea Drilling Project 90, 1347–1360, https://doi.org/10.2973/dsdp.proc.90.1986, 1986.

Naish, T. R., Woolfe, K. J., Barrett, P. J., Wilson, G. S., Atkins, C., Bohaty, S. M., Bücker, C. J., Claps, M., Davey, F. J., Dunbar, G. B., Dunn, A. G., Fielding, C. R., Florindo, F., Hannah, M. J., Harwood, D. M., Henrys, S. A., Krissek, L. A., Lavelle, M., van der Meer, J., McIntosh, W. C., Niessen, F., Passchier, S., Powell, R. D., Roberts, A. P., Sagnotti, L., Scherer, R. P., Strong, C. P., Talarico, F., Verosub, K. L., Villa, G., Watkins, D. K., Webb, P.-N., and Wonik, T.: Orbitally induced oscillations in the East Antarctic ice sheet at the Oligocene/Miocene boundary, Nature, 413, 719–723, https://doi.org/10.1038/35099534, 2001.

O'Brien, C. L., Robinson, S. A., Pancost, R. D., Sinninghe Damsté, J. S., Schouten, S., Lunt, D. J., Alsenz, H., Bornemann, A., Bottini, C., Brassell, S. C., Farnsworth, A., Forster, A., Huber, B. T., Inglis, G. N., Jenkyns, H. C., Linnert, C., Littler, K., Markwick, P., McAnena, A., Mutterlose, J., Naafs, B. D. A., Püttmann, W., Sluijs, A., van Helmond, N. A. G. M., Vellekoop, J., Wagner, T., and Wrobel, N. E.: Cretaceous sea-surface temperature evolution: Constraints from TEX86 and planktonic foraminiferal oxygen isotopes, Earth-Science Reviews, 172, 224–247, https://doi.org/10.1016/j.earscirev.2017.07.012, 2017.

O'Brien, C. L. ., Huber, M., Thomas, E., Pagani, M., Super, J. R., and Elder, L. E.: The enigma of Oligocene climate and global surface temperature evolution, Proceedings of the National Academy of Sciences of the United States of America, 117, 25302–25309, https://doi.org/10.1073/pnas.2003914117, 2020.

Pagani, M., Zachos, J. C., Freeman, K. H., Tipple, B., and Bohaty, S.: Marked Decline in Atmospheric Carbon Dioxide Concentrations During the Paleogene, Science, 309, 600–603, https://doi.org/10.1126/science.1110063, 2005.

Pagani, M., Huber, M., Liu, Z., Bohaty, S. M., Henderiks, J., Sijp, W., Krishnan, S., and DeConto, R. M.: The Role of Carbon Dioxide During the Onset of Antarctic Glaciation, Science, 334, 1261–1264, https://doi.org/10.1126/science.1203909, 2011.

Palaeosens Project Members: Making sense of palaeoclimate sensitivity, Nature, 491, 683–691, https://doi.org/10.1038/nature11574, 2012.

Palazzesi, L. and Barreda, V.: Major vegetation trends in the Tertiary of Patagonia (Argentina): A qualitative paleoclimatic approach based on palynological evidence, Flora: Morphology, Distribution, Functional Ecology of Plants, 202, https://doi.org/10.1016/j.flora.2006.07.006, 2007.

Palcu, D. V. and Krijgsman, W.: The dire straits of Paratethys: gateways to the anoxic giant of Eurasia, SP, 523, SP523-2021–73, https://doi.org/10.1144/SP523-2021-73, 2023.

Pälike, H., Frazier, J., and Zachos, J. C.: Extended orbitally forced palaeoclimatic records from the equatorial Atlantic Ceara Rise, Quaternary Science Reviews, 25, 3138–3149, https://doi.org/10.1016/j.quascirev.2006.02.011, 2006a.

Pälike, H., Norris, R. D., Herrle, J. O., Wilson, P. A., Coxall, H. K., Lear, C. H., Shackleton, N. J., Tripati, A. K., and Wade, B. S.: The heartbeat of the Oligocene climate system, Science, 314, 1894–1898, https://doi.org/10.1126/science.1133822, 2006b.

Pan, A. D.: The late Oligocene (28 - 27 Ma) Guang River Flora from the Northwestern Plateau of Ethiopia, University of California Santa Barbara, 2007.

Paull, R. and Hill, R. S.: Early oligocene Callitris and Fitzroya (Cupressaceae) from Tasmania, American Journal of Botany, 97, 809–820, https://doi.org/10.3732/ajb.0900374, 2010.

Pavlyutkin, B. I.: New species of thermophilic plants from the Early Oligocene flora of Kraskino (Primorski Region) as evidence of its subtropic type, Paleontol. J., 45, 698–704, https://doi.org/10.1134/S003103011106013X, 2011.

Pearson, P. N., Foster, G. L., and Wade, B. S.: Atmospheric carbon dioxide through the Eocene–Oligocene climate transition, Nature, 461, 1110–1113, https://doi.org/10.1038/nature08447, 2009.

Petersen, S. V. and Schrag, D. P.: Antarctic ice growth before and after the Eocene-Oligocene transition: New estimates from clumped isotope paleothermometry, Paleoceanography, 30, 1305–1317, https://doi.org/10.1002/2014PA002769, 2015.

Pierrehumbert, R. T., Brogniez, H., and Roca, R.: On the Relative Humidity of the Atmosphere, in: The Global Circulation of the Atmosphere, 143–185, 2002.

Plancq, J., Mattioli, E., Pittet, B., Simon, L., and Grossi, V.: Productivity and sea-surface temperature changes recorded during the late Eocene–early Oligocene at DSDP Site 511 (South Atlantic), Palaeogeography, Palaeoclimatology, Palaeoecology, 407, 34–44, https://doi.org/10.1016/j.palaeo.2014.04.016, 2014.

Pole, M., Hill, R., Green, N., and Macphail, M.: The Oligocene Berwick Quarry Flora — Rainforest in a Drying Environment, Aust. Systematic Bot., 6, 399–427, https://doi.org/10.1071/SB9930399, 1993.

Popov, S. V., Sychevskaya, E. K., Akhmet'ev, M. A., Zaporozhets, N. I., and Golovina, L. A.: Stratigraphy of the Maikop Group and Pteropoda Beds in northern Azerbaijan, Stratigr. Geol. Correl., 16, 664–677, https://doi.org/10.1134/S0869593808060063, 2008.

Prahl, F. G. and Wakeham, S. G.: Calibration of unsaturation patterns in long-chain ketone compositions for palaeotemperature assessment, Nature, 330, 367–369, https://doi.org/10.1038/330367a0, 1987.

Prebble, M., Sim, R., Finn, J., and Fink, D.: A Holocene Pollen and Diatom Record from Vanderlin Island, Gulf of Carpentaria, Lowland Tropical Australia, Quat. res., 64, 357–371, https://doi.org/10.1016/j.yqres.2005.08.005, 2005.

Rae, J. W. B., Zhang, Y. G., Liu, X., Foster, G. L., Stoll, H. M., and Whiteford, R. D. M.: Atmospheric CO_2 over the Past 66 Million Years from Marine Archives, Annu. Rev. Earth Planet. Sci., 49, 609–641, https://doi.org/10.1146/annurev-earth-082420-063026, 2021.

Raine, J. I. and Askin, R. A.: Terrestrial Palynology of Cape Roberts Project Drillhole CRP-3, Victoria Land Basin, Antarctica, Terra Antartica, 8, 389–400, 2001.

Raymo, M. E. and Ruddiman, W. F.: Tectonic forcing of late Cenozoic climate, Nature, 359, 117–122, https://doi.org/10.1038/359117a0, 1992.

Reichgelt, T., Baumgartner, A., Feng, R., and Willard, D. A.: Poleward amplification, seasonal rainfall and forest heterogeneity in the Miocene of the eastern USA, Global and Planetary Change, 222, 104073, https://doi.org/10.1016/j.gloplacha.2023.104073, 2023.

Rögl, V. F.: Palaeogeographic Considerations for Mediterranean and Paratethys Seaways (Oligocene to Miocene), Annalen des Naturhistorischen Museums in Wien, 99, 279–310, 1998.

Roth-Nebelsick, A., Oehm, C., Grein, M., Utescher, T., Kunzmann, L., Friedrich, J.-P., and Konrad, W.: Stomatal density and index data of Platanus neptuni leaf fossils and their evaluation as a CO2 proxy for the Oligocene, Review of Palaeobotany and Palynology, 206, 1–9, https://doi.org/10.1016/j.revpalbo.2014.03.001, 2014.

Salamy, K. A. and Zachos, J. C.: Latest Eocene-Early Oligocene climate change and Southern Ocean fertility: Inferences from sediment accumulation and stable isotope data, Palaeogeography, Palaeoclimatology, Palaeoecology, 145, 61–77, https://doi.org/10.1016/S0031-0182(98)00093-5, 1999.

Salard-Cheboldaeff, M.: Palynologie maestrichtienne et tertiaire du cameroun. Etude qualitative et repartition verticale des principales especes, Review of Palaeobotany and Palynology, 28, 365–388, https://doi.org/10.1016/0034-6667(79)90032-0, 1979.

Sangiorgi, F., Bijl, P. K., Passchier, S., Salzmann, U., Schouten, S., McKay, R., Cody, R. D., Pross, J., van de Flierdt, T., Bohaty, S. M., Levy, R., Williams, T., Escutia, C., and Brinkhuis, H.: Southern Ocean warming and Wilkes Land ice sheet retreat during the mid-Miocene, Nat Commun, 9, 317, https://doi.org/10.1038/s41467-017-02609-7, 2018.

Sauermilch, I., Whittaker, J. M., Klocker, A., Munday, D. R., Hochmuth, K., Bijl, P. K., and LaCasce, J. H.: Gateway-driven weakening of ocean gyres leads to Southern Ocean cooling, Nat Commun, 12, 6465, https://doi.org/10.1038/s41467-021-26658-1, 2021.

Scher, H. D. and Martin, E. E.: Timing and Climatic Consequences of the Opening of Drake Passage, Science, 312, 428–430, https://doi.org/10.1126/science.1120044, 2006.

Scher, H. D. and Martin, E. E.: Oligocene deep water export from the North Atlantic and the development of the Antarctic Circumpolar Current examined with neodymium isotopes, Paleoceanography, 23, https://doi.org/10.1029/2006PA001400, 2008.

Scher, H. D., Whittaker, J. M., Williams, S. E., Latimer, J. C., Kordesch, W. E. C., and Delaney, M. L.: Onset of Antarctic Circumpolar Current 30 million years ago as Tasmanian Gateway aligned with westerlies, Nature, 523, 580–583, https://doi.org/10.1038/nature14598, 2015.

Schouten, S., Hopmans, E. C., Schefuß, E., and Sinninghe Damsté, J. S.: Distributional variations in marine crenarchaeotal membrane lipids: a new tool for reconstructing ancient sea water temperatures?, Earth and Planetary Science Letters, 204, 265–274, https://doi.org/10.1016/S0012-821X(02)00979-2, 2002.

Schulz, H., Bechtel, A., and Sachsenhofer, R.: The birth of the Paratethys during the Early Oligocene: From Tethys to an ancient Black Sea analogue?, Global and Planetary Change, 49, 163–176, https://doi.org/10.1016/j.gloplacha.2005.07.001, 2005.

Scotese, C. and Wright, N. M.: PaleoDEM Resource, EarthByte, 2018.

Shackleton, N. J.: Attainment of Isotopic Equilibrium Between Ocean Water and the Benthic Formainifera genus Uvigerina: Isotopic Changes in the Ocean During the Last Glacial, Colloques Internationaux du C.N.R.S, 219, 203–209, https://doi.org/10013/epic.41396.d001, 1974.

Silva, I. P. and Jenkins, D. G.: Decision on the Eocene-Oligocene boundary stratotype, Episodes, 16, 379–382, https://doi.org/10.18814/epiiugs/1993/v16i3/002, 1993.

Śliwińska, K. K., Clausen, O. R., and Heilmann-Clausen, C.: A mid-Oligocene cooling (Oi-2b) reflected in the dinoflagellate record and in depositional sequence architecture. An integrated study from the eastern North Sea Basin, Marine and Petroleum Geology, 27, 1424–1430, https://doi.org/10.1016/j.marpetgeo.2010.03.008, 2010.

Sluiter, I. R. K., Holdgate, G. R., Reichgelt, T., Greenwood, D. R., Kershaw, A. P., and Schultz, N. L.: A new perspective on Late Eocene and Oligocene vegetation and paleoclimates of South-eastern Australia, Palaeogeography, Palaeoclimatology, Palaeoecology, 596, 110985, https://doi.org/10.1016/j.palaeo.2022.110985, 2022.

Solé, F., Fischer, V., Denayer, J., Speijer, R. P., Fournier, M., Le Verger, K., Ladevèze, S., Folie, A., and Smith, T.: The upper Eocene-Oligocene carnivorous mammals from the Quercy Phosphorites (France) housed in Belgian collections, Geol. Belg., 24, 1–16, https://doi.org/10.20341/gb.2020.006, 2020.

Spero, H. J. and Williams, D. F.: Extracting environmental information from planktonic foraminiferal δ13C data, Nature, 335, 717–719, https://doi.org/10.1038/335717a0, 1988.

Spero, H. J., Bijma, J., Lea, D. W., and Bemis, B. E.: Effect of seawater carbonate concentration on foraminiferal carbon and oxygen isotopes, Nature, 390, 497–500, https://doi.org/10.1038/37333, 1997.

Spicer, R. A., Farnsworth, A., and Su, T.: Cenozoic topography, monsoons and biodiversity conservation within the Tibetan Region: An evolving story, Plant Diversity, 42, 229–254, https://doi.org/10.1016/j.pld.2020.06.011, 2020.

Spicer, R. A., Su, T., Valdes, P. J., Farnsworth, A., Wu, F.-X., Shi, G., Spicer, T. E. V., and Zhou, Z.: The topographic evolution of the Tibetan Region as revealed by palaeontology, Palaeobio Palaeoenv, 101, 213–243, https://doi.org/10.1007/s12549-020-00452-1, 2021a.

Spicer, R. A., Su, T., Valdes, P. J., Farnsworth, A., Wu, F.-X., Shi, G., Spicer, T. E. V., and Zhou, Z.: Why 'the uplift of the Tibetan Plateau' is a myth, National Science Review, 8, nwaa091, https://doi.org/10.1093/nsr/nwaa091, 2021b.

St. John, K.: Cenozoic ice-rafting history of the central Arctic Ocean: Terrigenous sands on the Lomonosov Ridge, Paleoceanography, 23, 1–12, https://doi.org/10.1029/2007PA001483, 2008.

Steininger, F. F. and Wessely, G.: From the Tethyan Ocean to the Paratethys Sea: Oligocene to Neogene Stratigraphy, Paleogeography and Paleobiogeography of the circum-Mediterranean region and the Oligocene to Neogene Basin evolution in Austria, Mitt. Österr. Geol. Ges., 92, 95–116, 1999.

Steininger, F. F., Aubry, M. P., Berggren, W. A., Biolzi, M., M.Borsetti, A., Cartlidge, J. E., Cati, F., Corfield, R., Gelati, R., Iaccarino, S., Napoleone, C., Ottner, F., Rögl, F., Roetzel, R., Spezzaferri, S., Tateo, F., Villa, G., and Zevenboom, D.: The Global Stratotype Section and Point (GSSP) for the base of the Neogene, Episodes, 20, 23–28, https://doi.org/10.18814/epiiugs/1997/v20i1/005, 1997.

Steinthorsdottir, M., Coxall, H. K., De Boer, A. M., Huber, M., Barbolini, N., Bradshaw, C. D., Burls, N. J., Feakins, S. J., Gasson, E., Henderiks, J., Holbourn, A. E., Kiel, S., Kohn, M. J., Knorr, G., Kürschner, W. M., Lear, C. H., Liebrand, D., Lunt, D. J., Mörs, T., Pearson, P. N., Pound, M. J., Stoll, H., and Strömberg, C. A. E.: The Miocene: The Future of the Past, Paleoceanogr Paleoclimatol, 36, https://doi.org/10.1029/2020PA004037, 2021.

Stickley, C. E., Brinkhuis, H., Schellenberg, S. A., Sluijs, A., Röhl, U., Fuller, M., Grauert, M., Huber, M., Warnaar, J., and Williams, G. L.: Timing and nature of the deepening of the Tasmanian Gateway: DEEPENING OF THE TASMANIAN GATEWAY, Paleoceanography, 19, n/a-n/a, https://doi.org/10.1029/2004PA001022, 2004.

Stickley, C. E., St John, K., Koç, N., Jordan, R. W., Passchier, S., Pearce, R. B., and Kearns, L. E.: Evidence for middle Eocene Arctic sea ice from diatoms and ice-rafted debris, Nature, 460, 376–379, https://doi.org/10.1038/nature08163, 2009.

Su, T., Spicer, R. A., Li, S.-H., Xu, H., Huang, J., Sherlock, S., Huang, Y.-J., Li, S.-F., Wang, L., Jia, L.-B., Deng, W.-Y.-D., Liu, J., Deng, C.-L., Zhang, S.-T., Valdes, P. J., and Zhou, Z.-K.: Uplift, climate and biotic changes at the Eocene–Oligocene transition in south-eastern Tibet, National Science Review, 6, 495–504, https://doi.org/10.1093/nsr/nwy062, 2019.

Sun, J., Ni, X., Bi, S., Wu, W., Ye, J., Meng, J., and Windley, B. F.: Synchronous turnover of flora, fauna and climate at the Eocene–Oligocene Boundary in Asia, Sci Rep, 4, 1–6, https://doi.org/10.1038/srep07463, 2014.

Super, J. R., Thomas, E., Pagani, M., Huber, M., O'Brien, C. L., and Hull, P. M.: Miocene Evolution of North Atlantic Sea Surface Temperature, Paleoceanography and Paleoclimatology, 35, https://doi.org/10.1029/2019PA003748, 2020.

The Cenozoic CO2 Proxy Integration Project (CenCO2PIP) Consortium: Toward a Cenozoic history of atmospheric CO2, Science, 382, eadi5177, https://doi.org/10.1126/science.adi5177, 2023.

Thompson, N., Salzmann, U., López-Quirós, A., Bijl, P. K., Hoem, F. S., Etourneau, J., Sicre, M.-A., Roignant, S., Hocking, E., Amoo, M., and Escutia, C.: Vegetation change across the Drake Passage region linked to late Eocene cooling and glacial disturbance after the Eocene–Oligocene Transition, Vegetation Dynamics/Marine Archives/Cenozoic, https://doi.org/10.5194/cp-2021-84, 2021.

Tierney, J. E. and Tingley, M. P.: A Bayesian, spatially-varying calibration model for the TEX86 proxy, Geochimica et Cosmochimica Acta, 127, 83–106, https://doi.org/10.1016/j.gca.2013.11.026, 2014.

Tierney, J. E. and Tingley, M. P.: BAYSPLINE: A New Calibration for the Alkenone Paleothermometer, Paleoceanography and Paleoclimatology, 33, 281–301, https://doi.org/10.1002/2017PA003201, 2018.

Toggweiler, J. R. and Bjornsson, H.: Drake Passage and palaeoclimate, J. Quaternary Sci., 15, 319–328, https://doi.org/10.1002/1099-1417(200005)15:4<319::AID-JQS545>3.0.CO;2-C, 2000.

Tosal, A. and Martín-Closas, C.: Taphonomy and palaeoecology of the Oligocene flora from Cervera (Catalonia, Spain) and their implication in palaeoclimatic reconstruction, Review of Palaeobotany and Palynology, 233, 93–103, https://doi.org/10.1016/j.revpalbo.2016.06.008, 2016.

Toumoulin, A., Donnadieu, Y., Ladant, J. -B., Batenburg, S. J., Poblete, F., and Dupont-Nivet, G.: Quantifying the Effect of the Drake Passage Opening on the Eocene Ocean, Paleoceanography and Paleoclimatology, 35, https://doi.org/10.1029/2020PA003889, 2020.

Tremblin, M., Hermoso, M., and Minoletti, F.: Equatorial heat accumulation as a long-term trigger of permanent Antarctic ice sheets during the Cenozoic, Proceedings of the National Academy of Sciences, 113, 11782–11787, https://doi.org/10.1073/pnas.1608100113, 2016.

Tripati, A., Backman, J., Elderfield, H., and Ferretti, P.: Eocene bipolar glaciation associated with global carbon cycle changes, Nature, 436, 341–346, https://doi.org/10.1038/nature03874, 2005.

Van Simaeys, S.: The Rupelian-Chattian boundary in the North Sea Basin and its calibration to the international time-scale, Netherlands Journal of Geosciences, 83, 241–248, https://doi.org/10.1017/S0016774600020308, 2004.

Van Simaeys, S., Man, E. D., Vandenberghe, N., Brinkhuis, H., and Steurbaut, E.: Stratigraphic and palaeoenvironmental analysis of the Rupelian-Chattian transition in the type region: Evidence from dinoflagellate cysts, foraminifera and calcareous nannofossils, Palaeogeography, Palaeoclimatology, Palaeoecology, 208, 31–58, https://doi.org/10.1016/j.palaeo.2004.02.029, 2004.

Van Simaeys, S., Brinkhuis, H., Pross, J., Williams, G. L., and Zachos, J. C.: Arctic dinoflagellate migrations mark the strongest Oligocene glaciations, Geol, 33, 709–712, https://doi.org/10.1130/G21634.1, 2005.

Via, R. K. and Thomas, D. J.: Evolution of Atlantic thermohaline circulation: Early Oligocene onset of deep-water production in the North Atlantic, Geol, 34, 441–444, https://doi.org/10.1130/G22545.1, 2006.

Wang, C., Dai, J., Zhao, X., Li, Y., Graham, S. A., He, D., Ran, B., and Meng, J.: Outward-growth of the Tibetan Plateau during the Cenozoic: A review, Tectonophysics, 621, 1–43, https://doi.org/10.1016/j.tecto.2014.01.036, 2014.

van der Weijst, C. M. H., van der Laan, K. J., Peterse, F., Reichart, G.-J., Sangiorgi, F., Schouten, S., Veenstra, T. J. T., and Sluijs, A.: A 15-million-year surface- and subsurface-integrated TEX_{86} temperature record from the eastern equatorial Atlantic, Clim. Past, 18, 1947–1962, https://doi.org/10.5194/cp-18-1947-2022, 2022.

Westerhold, T., Marwan, N., Drury, A. J., Liebrand, D., Agnini, C., Anagnostou, E., Barnet, J. S. K., Bohaty, S. M., De Vleeschouwer, D., Florindo, F., Frederichs, T., Hodell, D. A., Holbourn, A. E., Kroon, D., Lauretano, V., Littler, K., Lourens, L. J., Lyle, M., Pälike, H., Röhl, U., Tian, J., Wilkens, R. H., Wilson, P. A., and Zachos, J. C.: An astronomically dated record of Earth's climate and its predictability over the last 66 million years, Science, 369, 1383–1387, https://doi.org/10.1126/science.aba6853, 2020.

Willard, D. A., Donders, T. H., Reichgelt, T., Greenwood, D. R., Sangiorgi, F., Peterse, F., Nierop, K. G. J., Frieling, J., Schouten, S., and Sluijs, A.: Arctic vegetation, temperature, and hydrology during Early Eocene transient global warming events, Global and Planetary Change, 178, 139–152, https://doi.org/10.1016/j.gloplacha.2019.04.012, 2019.

Winterberg, S., Picotti, V., and Willett, S. D.: Messinian or Pleistocene valley incision within the Southern Alps, Swiss J Geosci, 113, 7, https://doi.org/10.1186/s00015-020-00361-7, 2020.

Witkowski, C. R., Weijers, J. W. H., Blais, B., Schouten, S., and Sinninghe Damsté, J. S.: Molecular fossils from phytoplankton reveal secular *P* CO_2 trend over the Phanerozoic, Sci. Adv., 4, 1–8, https://doi.org/10.1126/sciadv.aat4556, 2018.

Wright, N. M., Scher, H. D., Seton, M., Huck, C. E., and Duggan, B. D.: No Change in Southern Ocean Circulation in the Indian Ocean From the Eocene Through Late Oligocene, Paleoceanography and Paleoclimatology, 33, 152–167, https://doi.org/10.1002/2017PA003238, 2018.

Wuchter, C., Schouten, S., Coolen, M. J. L., and Sinninghe Damsté, J. S.: Temperature-dependent variation in the distribution of tetraether membrane lipids of marine Crenarchaeota: Implications for TEX_{86} paleothermometry, Paleoceanography, 19, 1–10, https://doi.org/10.1029/2004PA001041, 2004.

Zachos, J. C., Quinn, T. M., and Salamy, K. A.: High-resolution deap-sea foraminiferal stable isotope records of the Eocene-Oligocene transition, Paleoceanography, 11, 251–266, 1996.

Zanazzi, A., Kohn, M. J., MacFadden, B. J., and Terry, D. O.: Large temperature drop across the Eocene–Oligocene transition in central North America, Nature, 445, 639–642, https://doi.org/10.1038/nature05551, 2007.

Zeebe, R. E., Bijma, J., and Wolf-Gladrow, D. A.: A diffusion-reaction model of carbon isotope fractionation in foraminifera, Marine Chemistry, 64, 199–227, https://doi.org/10.1016/S0304-4203(98)00075-9, 1999.

Zhang, Y. G., Pagani, M., Liu, Z., Bohaty, S. M., and DeConto, R.: A 40-million-year history of atmospheric CO_2, Phil. Trans. R. Soc. A., 371, 20130096, https://doi.org/10.1098/rsta.2013.0096, 2013.